

Pedagogical Review of the Mølmer-Sørensen Gate in the Adiabatic Regime

David Verran

September 2025

Abstract

This review presents a derivation and analysis of the core Mølmer-Sørensen (MS) gate dynamics in the regime of small Rabi frequencies and Lamb-Dicke factors, as well as symmetric detunings, Rabi frequency strengths, and phase. Under these assumptions, the Hamiltonian is derived from scratch, and a simple model for unitary evolution under it is derived using the Magnus expansion. Within this regime, we present an analysis of the key properties of the MS gate, and optimal tuning of the relevant experimental parameters for high fidelity is discussed. We extend this analysis further by presenting a crude derivation and analysis of the low-order dynamics obtained when pushing only slightly beyond the weak-driving regime, followed by a discussion of the major noise sources limiting fidelity and their resulting dynamics. We conclude with a construction of CNOT using the MS gate and single-qubit unitaries.

Contents

1	Introduction	2
2	Derivation of the Hamiltonian	2
3	Derivation of the Gate Dynamics	6
3.1	Derivation of the Evolution Operator	8
3.2	Obtaining the MS gate unitary	10
4	Analysis of the Gate Dynamics	12
5	Impact of Carrier Transition	16
5.1	Adiabatic Elimination of Carrier Transition Levels	17
5.2	Verification of Carrier Transition Effects	22
6	Other noise sources	24
6.1	Dynamics of open systems	24
6.2	Spontaneous Emission	26
6.3	Dephasing	28
6.4	Motional Heating	30
7	Construction of CNOT	35
8	Bibliography	37
A	Appendix	38
A.1	Von Neumann equation in the Interaction Picture	38
A.2	Displacement Operator in Phase-Space	38

1 Introduction

Universal quantum computation requires the ability to construct both single-qubit and entangling 2-qubit unitaries with high fidelity [1][4]. For trapped-ion processors, one of the most promising gate designs for 2-qubit entangling gates is the Mølmer-Sørensen (hereafter MS) gate. This gate has the remarkable property that it is insensitive to the motional state of the ions, which allows it to operate at finite temperature [3][4].

Since the original conception of this gate in 1999 by Anders Sørensen and Klaus Mølmer [2], there have been a number of efforts to improve the design, in particular to speed up the gate time without sacrificing fidelity [7][10]. This is of critical importance as slow gate speeds are perhaps the most significant hindrance to the trapped-ion architecture when compared to competing modalities such as superconducting qubits [4]. Despite boasting longer coherence times, better connectivity of qubits and better prospects for scalability, gate speeds have historically been limited to the microsecond range, in stark contrast to the nanosecond speeds offered by superconducting qubits and competing modalities [4]. If fast high-fidelity 2-qubit gates can be realised experimentally, this author believes that this will solidify trapped-ion qubits as the superior modality for quantum computing. Whilst the subject of pulse shaping and other efforts to increase gate speed are beyond the scope of this review, we mention here the current direction of research in this gate and what it promises to deliver, to stress its relevance and importance to the field of quantum computing, in order to motivate a thorough understanding of the core dynamics of the gate as presented in the following.

2 Derivation of the Hamiltonian

We begin with a detailed derivation of the Hamiltonian for a simple toy model of an ion trap. The trap will contain 2 identical ions, each of which will have some electronic energy level structure. We adopt here the 2-level picture where we assume the remaining energy eigenstates of the ion's internal Hamiltonian will be sufficiently off-resonant from any lasers we will later add, such that they do not contribute to the dynamics of the system. In practice, these off-resonant states will typically induce AC Stark shifts to the reduced 2-level system, but these will not be considered for the moment. The Hamiltonian of each ion will therefore be represented by some ground state $|g\rangle$ and some excited state $|e\rangle$ with energy $\hbar\omega_0$ above the ground state. These two states will form the computational basis states $|0\rangle$ and $|1\rangle$ for when we later use the trapped-ion system for quantum computation. This gives the following contribution to the Hamiltonian:

$$H_{\text{electronic}} = \hbar\omega_0|e\rangle\langle e| \otimes \mathbb{I} + \mathbb{I} \otimes \hbar\omega_0|e\rangle\langle e| \quad (1)$$

For simplicity, we will assume the two states $|g\rangle$ and $|e\rangle$ are dipole connected in this picture, although the same arguments will be applicable for higher order electric-quadrupole or magnetic-dipole connected states, or even for an effective Hamiltonian obtained from two-photon stimulated Raman transitions through some third virtual state.

When the ions are put into the trap, we must also allow for collective normal mode oscillations of the system. For 2 ions, there will be 2 modes (neglecting the transverse modes), but for the moment we assume that only one mode will be on-resonant whilst the other will not contribute to the dynamics. We therefore get a harmonic oscillator energy level structure at some trap frequency ν_0 :

$$H_{\text{motional}} = \hbar\nu_0\hat{a}^\dagger\hat{a}, \quad (2)$$

where \hat{a}^\dagger and \hat{a} are the creation and annihilation operators for the motional phonon mode at frequency ν_0 . Combining these two terms, we obtain the core Hamiltonian of the unperturbed system:

$$H_0 = H_{\text{electronic}} \otimes \mathbb{I}_{\text{motional}} + \mathbb{I}_{\text{electronic}} \otimes H_{\text{motional}} \quad (3)$$

The resulting energy level structure is shown in Figure 1:

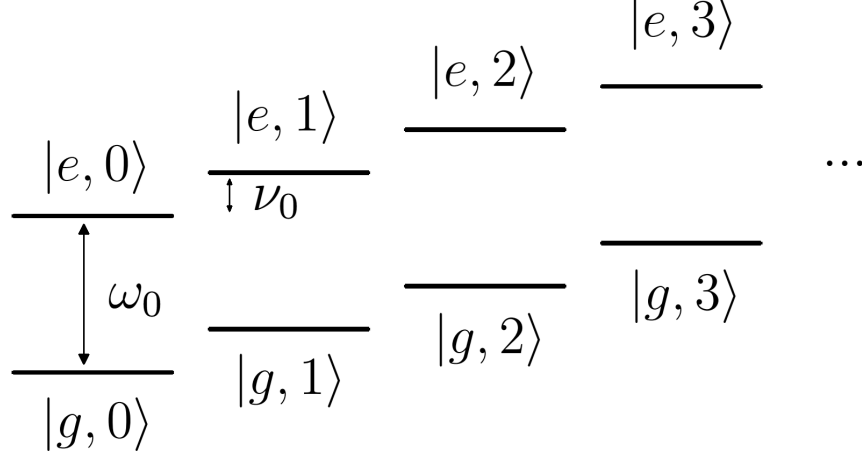


Figure 1: Energy level structure of H_0 in units of \hbar . The numbers denote the number of phonons in the motional subspace.

We now consider perturbing the ion trap system with 2 lasers. The lasers are for the moment assumed to be perfectly monochromatic at laser frequencies ω_{L1} and ω_{L2} . In the semi-classical picture, both ions will acquire dipole moments $-\hat{d} \cdot \vec{E}$. We therefore obtain a perturbation Hamiltonian:

$$\begin{aligned} H_{\text{int}} &= -\hat{d}_1 \cdot (\vec{E}_{L1}(z, t) + \vec{E}_{L2}(z, t)) \otimes \mathbb{I}_{\text{ion2}} \\ &\quad + \mathbb{I}_{\text{ion1}} \otimes -\hat{d}_2 \cdot (\vec{E}_{L1}(z, t) + \vec{E}_{L2}(z, t)) \\ &= \sum_{j=1}^{\#ions} \sum_{l=1}^{\#lasers} -\hat{d}_j \cdot \vec{E}_l(z, t) \end{aligned} \quad (4)$$

We take $\vec{E}_{L1} = E_0 \hat{x} \cos(k_{L1}z - \omega_{L1}t + \phi_{L1})$ and analogously for \vec{E}_{L2} . Note here we have implicitly assumed the two lasers have the same amplitude E_0 and thus their corresponding Rabi frequencies will be equivalent. Defining \vec{r}_1 to be the position of the valence electron of ion 1 relative to equilibrium and analogously for ion 2:

$$\begin{aligned} -\hat{d}_j \cdot \vec{E}_l &= e\vec{r}_j \cdot E_0 \hat{x} \cos(k_l z - \omega_l t + \phi_l) \\ &= \frac{e\hat{x}_j E_0}{2} (e^{i(k_l z - \omega_l t + \phi_l)} + e^{-i(k_l z - \omega_l t + \phi_l)}) \end{aligned} \quad (5)$$

In the 2-level picture, we express the operator \hat{x} in terms of the $\{|g\rangle, |e\rangle\}$ basis. For the dipole transitions considered here, selection rules will kill the diagonal elements via parity arguments, but we will find that similar arguments can be employed for the other cases (magnetic dipole, electric quadrupole, Raman) to yield:

$$\begin{aligned}\langle g|\hat{x}|g\rangle &= \langle e|\hat{x}|e\rangle = 0 \\ \langle g|\hat{x}|e\rangle &= \langle e|\hat{x}|g\rangle \in \mathbb{R} \text{ for bound states.}\end{aligned}\tag{6}$$

We define the Rabi frequency Ω_R as follows:

$$\hbar\Omega_R \equiv \langle g|e\hat{x}E_0|e\rangle,\tag{7}$$

such that the operator $eE_0\hat{x}$ can be expressed as:

$$\begin{aligned}eE_0\hat{x} &= (|e\rangle\langle e| + |g\rangle\langle g|)eE_0\hat{x}(|e\rangle\langle e| + |g\rangle\langle g|) \\ &= \hbar\Omega_R(|e\rangle\langle g| + |g\rangle\langle e|) \\ &= \hbar\Omega_R\hat{\sigma}_x,\end{aligned}\tag{8}$$

where $\hat{\sigma}_x$ is the Pauli x operator. Substituting this back into the interaction Hamiltonian H_{int} :

$$H_{int} = \sum_{j=1}^{\#ions} \sum_{l=1}^{\#lasers} \frac{\hbar\Omega_R}{2} (\hat{\sigma}_x^{(j)} e^{i(k_l z - \omega_l t + \phi_l)} + h.c.) \otimes \mathbb{I}_{\text{motional}},\tag{9}$$

where $h.c.$ denotes the Hermitian conjugate. We now take the approximation that each ion is never displaced very far from equilibrium relative to the wavelengths of the driving lasers. By taking the operator \hat{z} for each ion and recognising that we can represent this observable by $z_0(\hat{a} + \hat{a}^\dagger)$ (assuming that only this normal mode at frequency ν_0 is excited) for operators \hat{a} and \hat{a}^\dagger defined as above, we can formalise this assumption by taking the approximation that $kz_0 \ll 1$ for each laser mode k_{L1} and k_{L2} . This is the *Lamb-Dicke approximation*, and we can define the Lamb-Dicke factor $\eta \equiv kz_0$ to be some small parameter which we assume is roughly equivalent for each ion. This equivalency will hold true for the centre-of-mass mode of oscillations, such that all ions vibrate equally [6]. This allows us to expand the exponential $e^{ikz} \approx 1 + ikz$ such that:

$$H_{int} = \sum_{j=1}^{\#ions} \sum_{l=1}^{\#lasers} \frac{\hbar\Omega_R}{2} (\hat{\sigma}_x^{(j)} (1 + i\eta(\hat{a} + \hat{a}^\dagger)) e^{i(-\omega_l t + \phi_l)} + h.c.) \otimes \mathbb{I}_{\text{motional}} + O(\eta^2)\tag{10}$$

Lastly, it is common to move into an interaction picture rotating with the unperturbed Hamiltonian H_0 . This picture is useful in order that the computational basis states and different phonon states do not acquire phase relative to each other over time. To transform into the interaction frame, we make the mappings $\rho \rightarrow \tilde{\rho} \equiv \exp(\frac{iH_0 t}{\hbar}) \rho \exp(\frac{-iH_0 t}{\hbar})$ and $H_{int} \rightarrow \tilde{H}_{int} \equiv \exp(\frac{iH_0 t}{\hbar}) H_{int} \exp(\frac{-iH_0 t}{\hbar})$, where ρ is some density matrix evolving under the Hamiltonian $H_{tot} \equiv H_0 + H_{int}$. In this frame, the von Neumann equation $\frac{d}{dt}\rho = -\frac{i}{\hbar}[H_{tot}, \rho]$ can be shown to instead read $\frac{d}{dt}\tilde{\rho} = -\frac{i}{\hbar}[\tilde{H}_{int}, \tilde{\rho}]$, thus eliminating the phase accrual of the energy eigenstates of H_0 . A proof of this claim is provided in Appendix A.1. We therefore require \tilde{H}_{int} :

$$\tilde{H}_{int} = \exp(\frac{iH_0 t}{\hbar}) \sum_{j=1}^{\#ions} \sum_{l=1}^{\#lasers} \frac{\hbar\Omega_R}{2} (\hat{\sigma}_x^{(j)} (1 + i\eta(\hat{a} + \hat{a}^\dagger)) e^{i(-\omega_l t + \phi_l)} + h.c.) \exp(\frac{-iH_0 t}{\hbar})\tag{11}$$

For atomic eigenstates $\{|g\rangle, |e\rangle\}$, $\hat{\sigma}_x$ only has non-zero matrix elements connecting $|g\rangle$ to $|e\rangle$ and vice versa. By considering explicitly what happens in each case, we obtain:

$$\begin{aligned}\langle g|e^{\frac{iH_0t}{\hbar}}\hat{\sigma}_x^{(j)}e^{-\frac{iH_0t}{\hbar}}|e\rangle &= \langle g|\hat{\sigma}_x^{(j)}e^{-i\omega_0t}|e\rangle = e^{-i\omega_0t} \\ \langle e|e^{\frac{iH_0t}{\hbar}}\hat{\sigma}_x^{(j)}e^{-\frac{iH_0t}{\hbar}}|g\rangle &= \langle e|e^{i\omega_0t}\hat{\sigma}_x^{(j)}|g\rangle = e^{i\omega_0t} \\ \implies e^{\frac{iH_0t}{\hbar}}\hat{\sigma}_x^{(j)}e^{-\frac{iH_0t}{\hbar}} &= e^{i\omega_0t}\hat{\sigma}_+^{(j)} + e^{-i\omega_0t}\hat{\sigma}_-^{(j)}\end{aligned}\quad (12)$$

Similarly, for the motional space operators:

$$\begin{aligned}\langle n|e^{\frac{iH_0t}{\hbar}}\hat{a}e^{-\frac{iH_0t}{\hbar}}|n+1\rangle &= \langle n|e^{n\nu_0t}\hat{a}e^{-(n+1)\nu_0t}|n+1\rangle \\ &= \langle n|\hat{a}|n+1\rangle e^{-\nu_0t} \\ \langle n+1|e^{\frac{iH_0t}{\hbar}}\hat{a}^\dagger e^{-\frac{iH_0t}{\hbar}}|n\rangle &= \langle n+1|e^{(n+1)\nu_0t}\hat{a}^\dagger e^{-n\nu_0t}|n\rangle \\ &= \langle n+1|\hat{a}^\dagger|n\rangle e^{\nu_0t} \\ \implies e^{\frac{iH_0t}{\hbar}}(\hat{a} + \hat{a}^\dagger)e^{-\frac{iH_0t}{\hbar}} &= \hat{a}e^{-\nu_0t} + \hat{a}^\dagger e^{\nu_0t}\end{aligned}\quad (13)$$

Combining the above, we obtain for the interaction picture Hamiltonian:

$$\tilde{H}_{int} = \sum_{j=1}^{\#ions} \sum_{l=1}^{\#lasers} \frac{\hbar\Omega_R}{2} (e^{i\omega_0t}\hat{\sigma}_+^{(j)} + e^{-i\omega_0t}\hat{\sigma}_-^{(j)}) (1 + i\eta(\hat{a}e^{-\nu_0t} + \hat{a}^\dagger e^{\nu_0t})) e^{i(-\omega_l t + \phi_l)} + h.c. \quad (14)$$

At this stage it becomes instructive for the purposes of quantum computing to reorganise the terms to explicitly show the particular transitions we may want to excite to construct various gates:

$$\begin{aligned}\tilde{H}_{int} &= \sum_{j=1}^{\#ions} \sum_{l=1}^{\#lasers} \frac{\hbar\Omega_R}{2} (e^{i\omega_0t}\hat{\sigma}_+^{(j)} + e^{-i\omega_0t}\hat{\sigma}_-^{(j)}) e^{i(-\omega_l t + \phi_l)} + h.c. \\ &\quad + \frac{i\hbar\eta\Omega_R}{2} (e^{i\omega_0t}\hat{\sigma}_+^{(j)} + e^{-i\omega_0t}\hat{\sigma}_-^{(j)}) (\hat{a}e^{-\nu_0t} + \hat{a}^\dagger e^{\nu_0t}) e^{i(-\omega_l t + \phi_l)} + h.c. \\ &= \sum_{j=1}^{\#ions} \sum_{l=1}^{\#lasers} \frac{\hbar\Omega_R}{2} (e^{i\omega_0t}\hat{\sigma}_+^{(j)} + e^{-i\omega_0t}\hat{\sigma}_-^{(j)}) e^{i(-\omega_l t + \phi_l)} + h.c. \\ &\quad + \frac{i\hbar\eta\Omega_R}{2} (e^{i(\omega_0-\nu_0)t}\hat{\sigma}_+^{(j)}\hat{a} + e^{-i(\omega_0-\nu_0)t}\hat{\sigma}_-^{(j)}\hat{a}^\dagger) e^{i(-\omega_l t + \phi_l)} + h.c. \\ &\quad + \frac{i\hbar\eta\Omega_R}{2} (e^{i(\omega_0+\nu_0)t}\hat{\sigma}_+^{(j)}\hat{a}^\dagger + e^{-i(\omega_0+\nu_0)t}\hat{\sigma}_-^{(j)}\hat{a}) e^{i(-\omega_l t + \phi_l)} + h.c.\end{aligned}\quad (15)$$

Asserting now that the laser frequency detunings are chosen such that $\omega_l + \omega_0 \gg |\omega_l - \omega_0|$, where ω_0 gives the largest frequency scale in the system, we can make the rotating wave approximation (hereafter RWA) to kill off the far off-resonant terms:

$$\begin{aligned}
\tilde{H}_{int} = & \sum_{j=1}^{\#ions} \sum_{l=1}^{\#lasers} \frac{\hbar\Omega_R}{2} e^{i((\omega_0-\omega_l)t+\phi_l)} \hat{\sigma}_+^{(j)} + h.c. \\
& + \frac{i\hbar\eta\Omega_R}{2} e^{i((\omega_0-\nu_0-\omega_l)t+\phi_l)} \hat{\sigma}_+^{(j)} \hat{a} + h.c. \\
& + \frac{i\hbar\eta\Omega_R}{2} e^{i((\omega_0+\nu_0-\omega_l)t+\phi_l)} \hat{\sigma}_+^{(j)} \hat{a}^\dagger + h.c.
\end{aligned} \tag{16}$$

This form of the Hamiltonian is useful as it clearly separates the *carrier* and *sideband* transitions [3], which will be defined in the following. The first term of strength $\frac{\hbar\Omega_R}{2}$ and with only the $\hat{\sigma}_+$ and $\hat{\sigma}_-$ operators gives the *carrier* transition, which allows for transitions between the computational $|g\rangle$ and $|e\rangle$ states without changing the phonon subspace. The next two terms are the *sideband* terms, and are weaker by a factor of η , which we remind here is chosen to be small such that the previously made Lamb-Dicke approximation is valid. The first sideband term is the *red* sideband transition and induces transitions between $|g, n\rangle$ and $|e, n-1\rangle$ states, where n denotes some number of phonons. The second sideband term is the *blue* sideband transition, and induces transitions between $|g, n\rangle$ and $|e, n+1\rangle$ states. These transitions are shown in Figure 2:

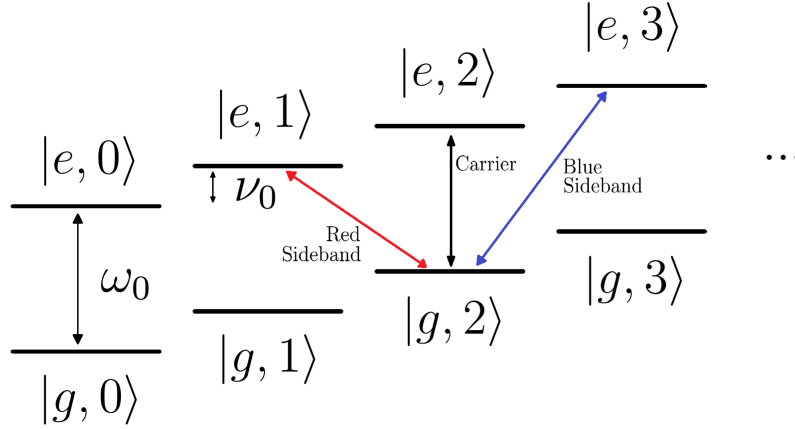


Figure 2: Carrier transition and the red and blue sideband transitions.

3 Derivation of the Gate Dynamics

In this section we derive the evolution operator for the Hamiltonian derived in Section 2 for the particular choice of laser frequencies and detunings as used in the MS gate. For the simplest toy model of the MS gate as worked through in the following, we fix the number of ions and the number of laser frequencies to 2. The goal is to obtain the following entangling gate:

$$U_{MS} = \frac{1}{\sqrt{2}} \begin{pmatrix} 1 & 0 & 0 & -i \\ 0 & 1 & -i & 0 \\ 0 & -i & 1 & 0 \\ -i & 0 & 0 & 1 \end{pmatrix}, \tag{17}$$

which we will later show is equivalent to a controlled phase C-Z gate (up to global single-qubit rotations).

Practically, this gate will be constructed by first achieving Rabi oscillations between the states $|gg\rangle$ and $|ee\rangle$, and between the states $|ge\rangle$ and $|eg\rangle$, then choosing the gate time such that we prematurely terminate the oscillation half-way. In this way, $|gg\rangle$ does not fully reach $|ee\rangle$, but we instead achieve the entangled state $\frac{1}{\sqrt{2}}(|gg\rangle - i|ee\rangle)$.

To construct Rabi oscillations in this way, the laser detunings are chosen such that we drive Raman transitions through the sidebands by only virtually exciting different phonon modes. In the simplest implementation of the MS gate, the laser frequencies $\omega_{L1} = \omega_0 - \nu_0 - \delta$ and $\omega_{L2} = \omega_0 + \nu_0 + \delta$ are chosen, where δ is a small detuning from the sidebands. Figure 3 shows how these detunings ensure that only the required transitions described above are Raman on-resonant:

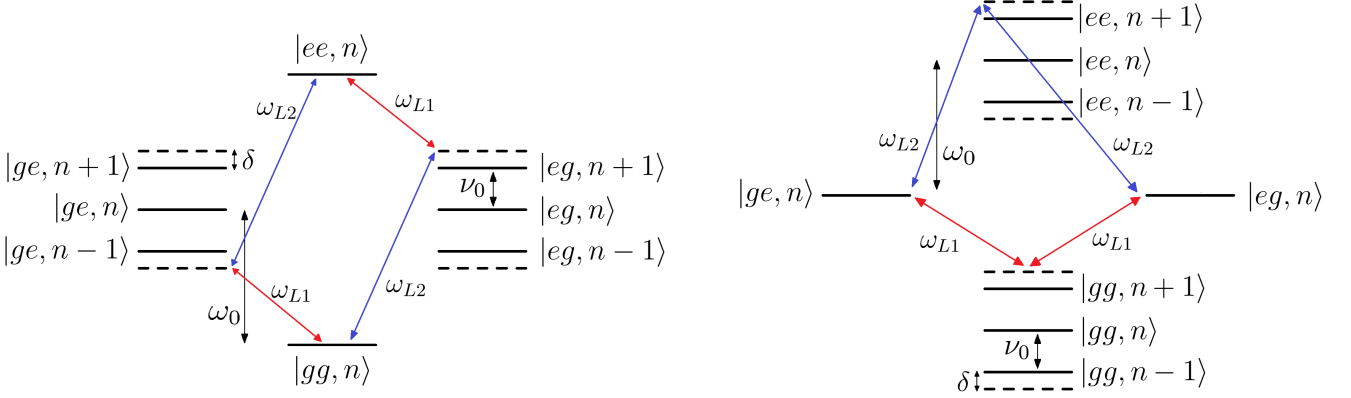


Figure 3: Raman transitions for MS gate. $|gg\rangle \longleftrightarrow |ee\rangle$ (left) and $|ge\rangle \longleftrightarrow |eg\rangle$ (right).

Substituting these values for ω_{L1} and ω_{L2} into the Hamiltonian derived in Section 2, and additionally taking symmetric phases $\phi_{L1} = \phi_{L2} = \phi$, we obtain:

$$\begin{aligned} \tilde{H}_{int} = & \sum_{j=1}^{\#ions} \frac{\hbar\Omega_R}{2} (e^{i((\nu_0+\delta)t+\phi)} + e^{i((- \nu_0-\delta)t+\phi)}) \hat{\sigma}_+^{(j)} + h.c. \\ & + \frac{i\hbar\eta\Omega_R}{2} (e^{i(\delta t+\phi)} + e^{i((-2\nu_0-\delta)t+\phi)}) \hat{\sigma}_+^{(j)} \hat{a} + h.c. \\ & + \frac{i\hbar\eta\Omega_R}{2} (e^{i((2\nu_0+\delta)t+\phi)} + e^{i(-\delta t+\phi)}) \hat{\sigma}_+^{(j)} \hat{a}^\dagger + h.c. \end{aligned} \quad (18)$$

At this point, a second RWA can be made to drop the fast oscillation terms. We will lose the carrier transition entirely, and keep only the red and blue sideband terms oscillating with frequency δ . This approximation will not necessarily be valid beyond the weak-driving regime, where Rabi frequencies are chosen to be larger in order to achieve faster gates. This is because although the carrier terms are off-resonant, they are larger by a factor of $\frac{1}{\eta}$ relative to the sidebands, and thus for sufficiently large Rabi frequencies relative to the detuning from the carrier $\nu_0 + \delta$, we will not be able to completely disregard its effects. We will discuss this regime further in Section 5. Nevertheless, for the simple setup we derive here, the second RWA is assumed to be valid for sufficiently large detunings $\nu_0 + \delta$. This yields the Hamiltonian:

$$\tilde{H}_{int} = \sum_{j=1}^{\#ions} \frac{i\hbar\eta\Omega_R e^{i\phi}}{2} \hat{\sigma}_+^{(j)} (e^{i\delta t} \hat{a} + e^{-i\delta t} \hat{a}^\dagger) + h.c. \quad (19)$$

For notational convenience, it is often useful to re-express $\hat{S}_+ \equiv \sum_{j=1}^{\#ions} \hat{\sigma}_+^{(j)}$, and additionally, to absorb the phase ϕ into \hat{S}_+ such that we can define $\hat{S}_+^{(\phi)} \equiv \hat{S}_+ e^{i\phi}$. Substituting into (19), we obtain:

$$\tilde{H}_{int} = \frac{i\hbar\eta\Omega_R}{2} \hat{S}_+^{(\phi)} (e^{i\delta t} \hat{a} + e^{-i\delta t} \hat{a}^\dagger) + h.c. \quad (20)$$

Lastly, by noting that $i\hat{\sigma}_+ + h.c. = -\hat{\sigma}_y$, we can analogously define $-\hat{S}_y^{(\phi)} \equiv i\hat{S}_+^{(\phi)} + h.c.$, which allows us to later exploit properties of Pauli matrices to ease calculations. Crucially, we find that $\hat{\sigma}_y^{(\phi)}$ will share similar properties to the standard $\hat{\sigma}_y$ operator, most notably:

$$\begin{aligned} \hat{\sigma}_y^{(\phi)2} &\equiv (-i\hat{\sigma}_+^{(\phi)} + i\hat{\sigma}_-^{(\phi)})^2 \\ &= (-i\hat{\sigma}_+ e^{i\phi} + i\hat{\sigma}_- e^{-i\phi})^2 \\ &= \hat{\sigma}_+ \hat{\sigma}_- e^{i(\phi-\phi)} + \hat{\sigma}_- \hat{\sigma}_+ e^{i(-\phi+\phi)} \\ &= \mathbb{I}. \end{aligned} \quad (21)$$

This final substitution yields our final form for the simplified MS Hamiltonian:

$$\tilde{H}_{int} = -\frac{\hbar\eta\Omega_R}{2} \hat{S}_y^{(\phi)} (e^{i\delta t} \hat{a} + e^{-i\delta t} \hat{a}^\dagger) \quad (22)$$

We are now ready to derive the form of the evolution operator.

3.1 Derivation of the Evolution Operator

In the following we solve for the evolution operator $U(t)$, defined by the time-evolution equation:

$$|\Psi(t)\rangle = U(t)|\Psi(t_0)\rangle \quad (23)$$

The evolution operator can be obtained from the Schrodinger equation:

$$i\hbar \frac{\partial}{\partial t} U(t) = H(t)U(t) \quad (24)$$

Unfortunately, the form of the Hamiltonian $\tilde{H}_{int}(t)$ for the trapped-ion system makes direct integration of this equation to find a solution for $U(t)$ impossible. This is because the commutator $[\tilde{H}(t_1), \tilde{H}(t_2)]$ for two different times t_1 and t_2 does not vanish in general, thus simply exponentiating the integral of $\tilde{H}(t)$ does not work in this case.

One possible solution is to instead use the *Magnus expansion*, where we assume a solution exists for the evolution operator $U(t)$ of the form $\exp(\Omega(t))$, where $\Omega(t)$ is found from a series expansion:

$$\Omega(t) = \Omega_1(t) + \Omega_2(t) + \Omega_3(t) + \dots \quad (25)$$

This expansion is useful as any premature truncation at finite order will still yield a unitary approximation due to the exponential structure, which in general will not be true for alternative methods such as the Dyson Series. A more in-depth discussion of the Magnus expansion including convergence properties can be found in [8].

The first few terms of the Magnus expansion are given by:

$$\begin{aligned}
\Omega_1(t) &= -\frac{i}{\hbar} \int_{t_0}^t dt_1 H(t_1) \\
\Omega_2(t) &= -\frac{1}{2\hbar^2} \int_{t_0}^t dt_1 \int_{t_0}^{t_1} dt_2 [H(t_1), H(t_2)] \\
\Omega_3(t) &= \frac{i}{6\hbar^3} \int_{t_0}^t dt_1 \int_{t_0}^{t_1} dt_2 \int_{t_0}^{t_2} dt_3 ([H(t_1), [H(t_2), H(t_3)]] + [H(t_3), [H(t_2), H(t_1)]])
\end{aligned} \tag{26}$$

We apply this to the MS Hamiltonian (22):

$$\begin{aligned}
\Omega_1(t) &= -\frac{i}{\hbar} \int_0^t dt_1 \tilde{H}(t_1) \\
&= \frac{i}{\hbar} \int_0^t dt_1 \frac{\hbar \eta \Omega_R}{2} \hat{S}_y^{(\phi)} (e^{i\delta t_1} \hat{a} + e^{-i\delta t_1} \hat{a}^\dagger) \\
&= \frac{i\eta \Omega_R}{2} \hat{S}_y^{(\phi)} \left(\frac{1}{i\delta} (e^{i\delta t} - 1) \hat{a} - \frac{1}{i\delta} (e^{-i\delta t} - 1) \hat{a}^\dagger \right) \\
&= \frac{\eta \Omega_R}{2\delta} \hat{S}_y^{(\phi)} ((e^{i\delta t} - 1) \hat{a} - (e^{-i\delta t} - 1) \hat{a}^\dagger)
\end{aligned} \tag{27}$$

In order to obtain $\Omega_2(t)$, it is first necessary to find an expression for the commutator of $\tilde{H}_{int}(t)$ with itself at different times:

$$\begin{aligned}
[\tilde{H}_{int}(t_1), \tilde{H}_{int}(t_2)] &= \left[-\frac{\hbar \eta \Omega_R}{2} \hat{S}_y^{(\phi)} (e^{i\delta t_1} \hat{a} + e^{-i\delta t_1} \hat{a}^\dagger), -\frac{\hbar \eta \Omega_R}{2} \hat{S}_y^{(\phi)} (e^{i\delta t_2} \hat{a} + e^{-i\delta t_2} \hat{a}^\dagger) \right] \\
&= \left(\frac{\hbar \eta \Omega_R}{2} \right)^2 \hat{S}_y^{(\phi)2} (e^{i\delta(t_1-t_2)} [\hat{a}, \hat{a}^\dagger] + e^{-i\delta(t_1-t_2)} [\hat{a}^\dagger, \hat{a}]) \\
&= \left(\frac{\hbar \eta \Omega_R}{2} \right)^2 \hat{S}_y^{(\phi)2} (e^{i\delta(t_1-t_2)} - e^{-i\delta(t_1-t_2)}) \otimes \mathbb{I}_{\text{motional}} \\
&= \left(\frac{\hbar \eta \Omega_R}{2} \right)^2 \hat{S}_y^{(\phi)2} \cdot 2i \sin(\delta(t_1 - t_2))
\end{aligned} \tag{28}$$

Substituting this into the second Magnus expansion term $\Omega_2(t)$:

$$\begin{aligned}
\Omega_2(t) &= -\frac{1}{2\hbar^2} \int_{t_0}^t dt_1 \int_{t_0}^{t_1} dt_2 [H(t_1), H(t_2)] \\
&= -\frac{1}{2\hbar^2} \int_0^t dt_1 \int_{t_0}^{t_1} dt_2 \left(\frac{\hbar \eta \Omega_R}{2} \right)^2 \hat{S}_y^{(\phi)2} \cdot 2i \sin(\delta(t_1 - t_2)) \\
&= -i \left(\frac{\eta \Omega_R}{2} \right)^2 \hat{S}_y^{(\phi)2} \int_{t_0}^t dt_1 \frac{1}{\delta} (1 - \cos(\delta t_1)) \\
&= -i \left(\frac{\eta \Omega_R}{2\delta} \right)^2 \hat{S}_y^{(\phi)2} (\delta t - \sin(\delta t))
\end{aligned} \tag{29}$$

Remarkably, as the commutator of $\tilde{H}_{int}(t)$ with itself at different times goes like $\hat{S}_y^{(\phi)2} \otimes \mathbb{I}_{\text{motional}}$, we obtain that $[\tilde{H}_{int}(t_1), [\tilde{H}_{int}(t_2), \tilde{H}_{int}(t_3)]] = 0$, and by extension all higher order commutators will also conveniently vanish. Thus, the Magnus expansion to only second order will give us an exact

evolution operator for $\tilde{H}_{int}(t)$. Note however, it is worth stating again that this does not mean we have solved for the exact MS gate dynamics, as the Hamiltonian used here was obtained after 2 rotating wave approximations, the second of which may not necessarily be valid. Further, noise effects including (but not limited to) spontaneous emission, stray magnetic fields, heating, as well as other off-resonant states of the ions have not been accounted for (we will discuss these in more detail in Section 6). Nevertheless, within the regime of well-isolated, long coherence time trapped-ions well within the Lamb-Dicke regime and with small Rabi frequencies, these two terms are sufficient to give an accurate representation of the gate dynamics we should expect. The final step is to combine them and obtain the evolution operator $U(t)$:

$$\begin{aligned}
U(t) &= \exp(\Omega_1(t) + \Omega_2(t)) \\
&= \exp(\Omega_1(t)) \cdot \exp(\Omega_2(t)) \quad (\text{as } \Omega_1(t) \text{ and } \Omega_2(t) \text{ commute}) \\
&= \exp\left(\frac{\eta\Omega_R}{2\delta}\hat{S}_y^{(\phi)}((e^{i\delta t} - 1)\hat{a} - (e^{-i\delta t} - 1)\hat{a}^\dagger)\right) \cdot \exp\left(-i\left(\frac{\eta\Omega_R}{2\delta}\right)^2\hat{S}_y^{(\phi)2}(\delta t - \sin(\delta t))\right)
\end{aligned} \tag{30}$$

3.2 Obtaining the MS gate unitary

We will now choose parameters δ and Ω_R such that at the gate time t_g , we obtain the MS gate unitary given in (17). The first term in (30) given by $\exp(\Omega_1(t))$ is typically referred to as the *displacement operator* [7], and is responsible for the motion of the phonon states in phase-space. This motion is unwanted for the entangling MS gate we want to obtain, as if we are not careful, it will generate residual correlations between the electronic qubit and motional subspaces at the gate time. We will therefore want to eliminate its contribution. By inspection, we immediately see that taking $\delta t_g = 2\pi m$ for $m \in \mathbb{Z}$ will cause $\exp(\Omega_1(t_g))$ to just give the identity. Additionally, this causes the second term to lose the contribution from $\sin(\delta t)$, as this will equal zero. The process of choosing the detuning in this way is called the *loop closure* condition, as we will later find that it is equivalent to ensuring that all phonon trajectories in phase-space form closed loops and return to their original state at the gate time.

A deeper discussion of the behaviour of this first term and the phase-space interpretation of the resulting motional space dynamics will be provided in Section 4, but for the moment we will proceed with the assumption that its contribution has been entirely eliminated at the gate time. Enforcing this condition on (30), we therefore obtain a much simpler form for the evolution operator:

$$U(t_g) = \exp\left(-i\delta t_g\left(\frac{\eta\Omega_R}{2\delta}\right)^2\hat{S}_y^{(\phi)2}\right) \tag{31}$$

To exponentiate this matrix, we note that $\hat{S}_y^{(\phi)2}$ has the following useful property:

$$\begin{aligned}
\hat{S}_y^{(\phi)2} &= (\hat{\sigma}_y^{(\phi)} \otimes \mathbb{I} + \mathbb{I} \otimes \hat{\sigma}_y^{(\phi)})^2 \\
&= (\hat{\sigma}_y^{(\phi)2} \otimes \mathbb{I}^2 + 2\hat{\sigma}_y^{(\phi)} \otimes \hat{\sigma}_y^{(\phi)} + \mathbb{I}^2 \otimes \hat{\sigma}_y^{(\phi)2}) \\
&= 2(\mathbb{I} \otimes \mathbb{I} + \hat{\sigma}_y^{(\phi)} \otimes \hat{\sigma}_y^{(\phi)})
\end{aligned} \tag{32}$$

$$\begin{aligned}
(\hat{S}_y^{(\phi)2})^2 &= 4(\mathbb{I}^2 \otimes \mathbb{I}^2 + 2\hat{\sigma}_y^{(\phi)} \otimes \hat{\sigma}_y^{(\phi)} + \hat{\sigma}_y^{(\phi)2} \otimes \hat{\sigma}_y^{(\phi)2}) \\
&= 4 \cdot 2(\mathbb{I} \otimes \mathbb{I} + \hat{\sigma}_y^{(\phi)} \otimes \hat{\sigma}_y^{(\phi)}) \\
&= 4\hat{S}_y^{(\phi)2}
\end{aligned} \tag{33}$$

And thus,

$$\left(\frac{1}{4}\hat{S}_y^{(\phi)2}\right)^n = \frac{1}{4}\hat{S}_y^{(\phi)2} \quad \forall n \in \mathbb{Z} \quad (34)$$

This allows us to express the exponential in a more convenient form:

$$\begin{aligned} U(t_g) &= \exp(-i\delta t_g \left(\frac{\eta\Omega_R}{2\delta}\right)^2 \hat{S}_y^{(\phi)2}) \\ &= \exp(-it_g \frac{\eta^2\Omega_R^2}{\delta} \frac{1}{4}\hat{S}_y^{(\phi)2}) \\ &= \mathbb{I} + (-it_g \frac{\eta^2\Omega_R^2}{\delta}) \left(\frac{1}{4}\hat{S}_y^{(\phi)2}\right) + \frac{1}{2}(-it_g \frac{\eta^2\Omega_R^2}{\delta})^2 \left(\frac{1}{4}\hat{S}_y^{(\phi)2}\right)^2 + \dots \\ &= \mathbb{I} - \left(\frac{1}{4}\hat{S}_y^{(\phi)2}\right) + \left(\frac{1}{4}\hat{S}_y^{(\phi)2}\right) \left(\mathbb{I} + (-it_g \frac{\eta^2\Omega_R^2}{\delta}) + \frac{1}{2}(-it_g \frac{\eta^2\Omega_R^2}{\delta})^2 + \dots\right) \\ &= \mathbb{I} - \left(\frac{1}{4}\hat{S}_y^{(\phi)2}\right) + \exp(-it_g \frac{\eta^2\Omega_R^2}{\delta}) \left(\frac{1}{4}\hat{S}_y^{(\phi)2}\right) \end{aligned} \quad (35)$$

At this point it becomes convenient to define the effective Rabi frequency for the MS gate oscillations $\Omega \equiv \frac{\eta^2\Omega_R^2}{2\delta}$. To obtain the final form of the MS gate, we re-express (35) in matrix form for ease of manipulation. For this, we require the matrix representing $\hat{S}_y^{(\phi)2}$:

$$\begin{aligned} \hat{S}_y^{(\phi)2} &= 2(\mathbb{I} \otimes \mathbb{I} + \hat{\sigma}_y^{(\phi)} \otimes \hat{\sigma}_y^{(\phi)}) \text{ (from (32))} \\ &= 2(\mathbb{I} \otimes \mathbb{I} + \begin{pmatrix} 0 & -ie^{i\phi} \\ ie^{-i\phi} & 0 \end{pmatrix} \otimes \begin{pmatrix} 0 & -ie^{i\phi} \\ ie^{-i\phi} & 0 \end{pmatrix}) \\ &= 2 \begin{pmatrix} 1 & 0 & 0 & 0 \\ 0 & 1 & 0 & 0 \\ 0 & 0 & 1 & 0 \\ 0 & 0 & 0 & 1 \end{pmatrix} + 2 \begin{pmatrix} 0 & 0 & 0 & -e^{2i\phi} \\ 0 & 0 & 1 & 0 \\ 0 & 1 & 0 & 0 \\ -e^{-2i\phi} & 0 & 0 & 0 \end{pmatrix} \\ &= 2 \begin{pmatrix} 1 & 0 & 0 & -e^{2i\phi} \\ 0 & 1 & 1 & 0 \\ 0 & 1 & 1 & 0 \\ -e^{-2i\phi} & 0 & 0 & 1 \end{pmatrix} \end{aligned} \quad (36)$$

Substituting this expression into $U(t_g)$, we obtain:

$$\begin{aligned} U(t_g) &= \begin{pmatrix} 1 & 0 & 0 & 0 \\ 0 & 1 & 0 & 0 \\ 0 & 0 & 1 & 0 \\ 0 & 0 & 0 & 1 \end{pmatrix} - \frac{1}{2} \begin{pmatrix} 1 & 0 & 0 & -e^{2i\phi} \\ 0 & 1 & 1 & 0 \\ 0 & 1 & 1 & 0 \\ -e^{-2i\phi} & 0 & 0 & 1 \end{pmatrix} + \frac{1}{2} \begin{pmatrix} 1 & 0 & 0 & -e^{2i\phi} \\ 0 & 1 & 1 & 0 \\ 0 & 1 & 1 & 0 \\ -e^{-2i\phi} & 0 & 0 & 1 \end{pmatrix} e^{-2i\Omega t_g} \\ &= \frac{1}{2} \begin{pmatrix} 1 + e^{-2i\Omega t_g} & 0 & 0 & e^{2i\phi}(1 - e^{-2i\Omega t_g}) \\ 0 & 1 + e^{-2i\Omega t_g} & e^{-2i\Omega t_g} - 1 & 0 \\ 0 & e^{-2i\Omega t_g} - 1 & 1 + e^{-2i\Omega t_g} & 0 \\ e^{-2i\phi}(1 - e^{-2i\Omega t_g}) & 0 & 0 & 1 + e^{-2i\Omega t_g} \end{pmatrix} \\ &= e^{-i\Omega t_g} \begin{pmatrix} \cos(\Omega t_g) & 0 & 0 & ie^{2i\phi}\sin(\Omega t_g) \\ 0 & \cos(\Omega t_g) & -i\sin(\Omega t_g) & 0 \\ 0 & -i\sin(\Omega t_g) & \cos(\Omega t_g) & 0 \\ ie^{-2i\phi}\sin(\Omega t_g) & 0 & 0 & \cos(\Omega t_g) \end{pmatrix} \end{aligned} \quad (37)$$

To achieve only half-way Rabi oscillations, we take $\Omega t_g = \frac{\pi}{4}$:

$$U(t_g) = \frac{1}{\sqrt{2}} \begin{pmatrix} 1 & 0 & 0 & ie^{2i\phi} \\ 0 & 1 & -i & 0 \\ 0 & -i & 1 & 0 \\ ie^{-2i\phi} & 0 & 0 & 1 \end{pmatrix}, \quad (38)$$

up to a global phase. For a choice of $\phi = \frac{\pi}{2}$, we obtain the entangling MS gate unitary presented in (17).

4 Analysis of the Gate Dynamics

The derivation in Section 3 enforces a number of conditions on the parameters involved in order that our gate achieves the required mappings at high fidelity. This section discusses how these conditions can be satisfied simultaneously, and provides an analysis of the resulting dynamics in both the motional and electronic qubit subspaces. In particular, we will focus our attention to the motional states of the ions, and we will present a mathematical framework to allow us to analyse their dynamics in phase-space. In order to obtain values for realistic gate times and to put into context the theoretical framework built up thus far, we will also later instantiate our toy model with a particular choice of physical implementation of trapped-ion qubits.

We list here the requirements derived above (not a comprehensive list) that need to be fulfilled:

- We require $\eta\sqrt{n} \ll 1$ in order that we are in the Lamb-Dicke regime and can disregard terms of order η^2 .
- We require that $\frac{\Omega_R}{\delta + \nu_0} \ll 1$ such that we remain in the weak-driving regime and can justify applying the second RWA to the carrier transitions. This condition and its violation will be discussed in more detail in Section 5.
- We require symmetric detunings δ from the two sideband transitions, as well as equal Rabi frequency strengths between the two laser frequencies. This is necessary to prevent any AC Stark shifts that will alter the phase accrual of the logical states.
- We require that the phases of the lasers be equivalent. For the particular choice of entangling gate we derived in Section 3, we additionally take $\phi = \frac{\pi}{2}$ to achieve the mappings $|gg\rangle \rightarrow \frac{1}{\sqrt{2}}(|gg\rangle - i|ee\rangle)$ and analogously for $|ee\rangle$. Note (38) implies that the mappings of $|ge\rangle$ and $|eg\rangle$ are insensitive to the particular choice of ϕ , assuming they are the same for both lasers.
- We require that the loop closure condition $\delta t_g = 2\pi m$ for $m \in \mathbb{Z}$ be fulfilled, such that the gate is insensitive to the motional state of the ions.
- Lastly, we require that the gate time t_g is chosen such that the Rabi oscillations at frequency $\Omega \equiv \frac{\Omega_R^2 \eta^2}{2\delta}$ are stopped half-way on the trajectory around the Bloch sphere from $|gg\rangle$ to $|ee\rangle$, and analogously for the other 3 2-qubit logical states.

It is worth stating that the conditions derived above may be violated intentionally when going beyond the weak-driving regime in the interests of counteracting additional errors that may arise here. For example, it is common to deliberately choose imbalances in the individual laser Rabi frequencies to create AC Stark shifts, which can be used to cancel other experimental sources of AC Stark shifts due to off-resonant scattering [6][11].

Interestingly, we find that following the loop closure condition, we lose all dependence on the motional state of the ions in the propagator $U(t_g)$ given in (31). By consequence, this means that in addition to allowing for any initial number of phonons (provided we remain firmly in the Lamb-Dicke regime), this insensitivity to the motional subspace is more powerful in that we also allow for any general superposition state of different numbers of phonons. This is one of the most appealing properties of the MS gate architecture, and one that makes it superior to its predecessor, the Cirac-Zoller gate, which only works correctly when the system is cooled to having exactly zero phonons [3]. In contrast, the analysis in Section 3 implies that the MS gate should still be able to operate with high fidelity even at finite temperature [3][4].

The final two conditions discussing the loop closure condition and the gate timing can be combined to give the following requirement on δ :

$$\begin{aligned} 2\pi \frac{\delta^2}{\Omega_R^2 \eta^2} &= 2\pi m \\ \implies \delta &= 2\Omega_R \eta \sqrt{m} \end{aligned} \tag{39}$$

Common choices of m are typically small integers in the range of 1-4, which is motivated by keeping δ as small as possible [2]. As the effective Rabi frequency for the MS gate oscillations scales $\sim \frac{1}{\delta}$, smaller detunings are motivated largely by a desire to construct faster gates. Further, for larger δ , it becomes experimentally harder to set the gate time t_g exactly to satisfy loop closure, as small offsets in timings could result in a large phase δt .

Figures 4 and 5 show plots of the Rabi oscillations obtained for the transition between $|gg\rangle$ and $|ee\rangle$ with and without the loop closure condition being satisfied respectively. We find, as expected, that the fidelities obtained with loop closure are much higher than those obtained without. The model parameters are taken from the setup described in [11], where the qubit is taken to be two quadrupole-connected levels of the $^{40}\text{Ca}^+$ ion. The energy splitting $\hbar\omega_0$ for these states is in the optical range with wavelength 729nm, thus qubits such as these are referred to as 'optical qubits'. The setup in [11] uses a linear Paul trap operating such that the axial centre-of-mass mode will have frequency $\nu_0 = 1\text{MHz}$, and the global beam for MS gate operation has Lamb-Dicke factor $\eta = 0.06$.

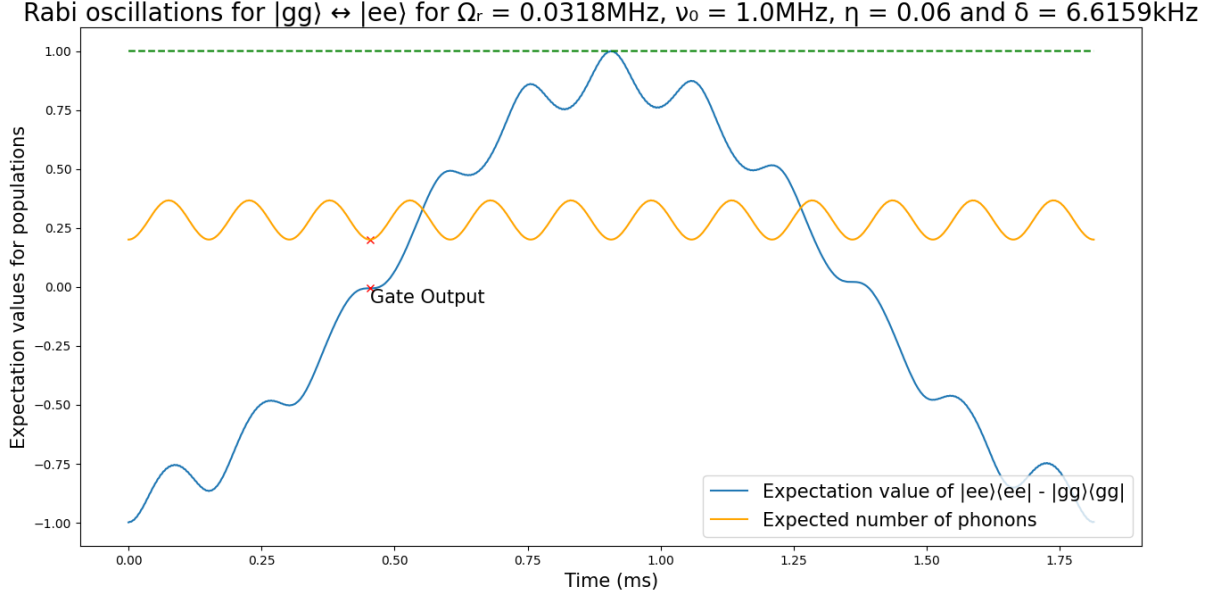


Figure 4: Rabi oscillations for $|gg\rangle \leftrightarrow |ee\rangle$ transitions for one cycle. The detuning δ is given by (39) with a choice of $m = 3$. This plot was produced for the parameters given in the graph title using a numerical Lindblad master equation solver in QuTip. The whole simulation can be found on my [GitHub page](#) under the name of MS gate.py. The orange line gives phonon oscillations governed by the displacement operator, with an initial motional state given by a thermal density matrix with an average number of phonons of 0.2. We note that at the gate time (red x), the oscillations return to its original value, as required. Without applying any rotating wave approximations and just using the raw Hamiltonian as given by (15), we obtain a fidelity for this mapping of $|gg\rangle \rightarrow \frac{1}{\sqrt{2}}(|gg\rangle - i|ee\rangle)$ of 0.99991.

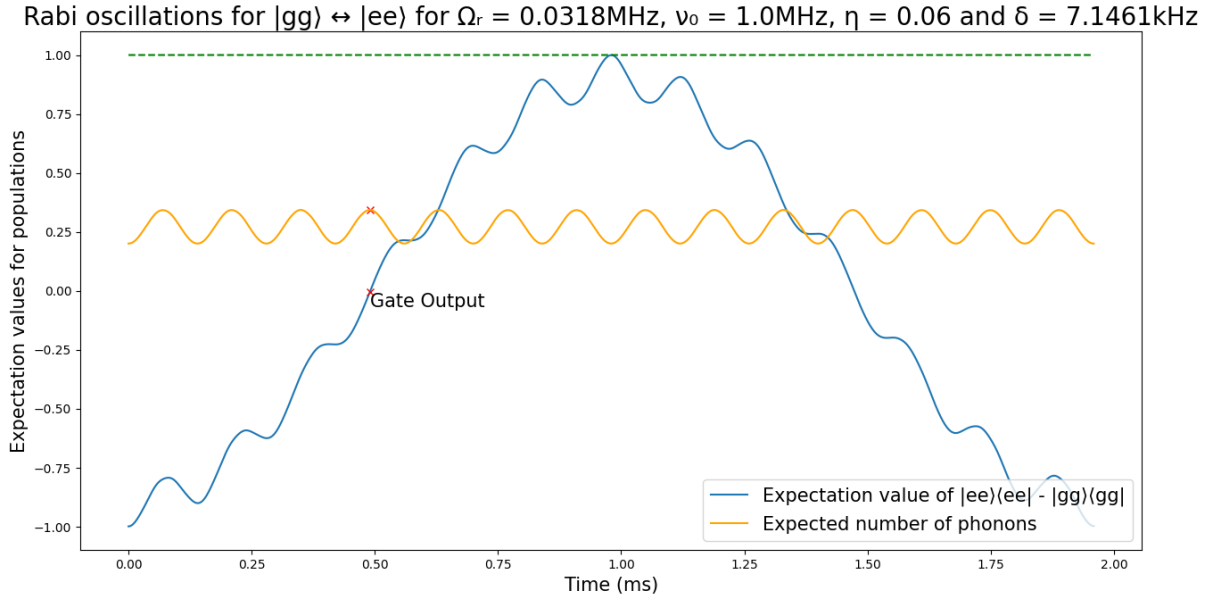


Figure 5: The same setup as in Figure 4, but with a non-integer choice of $m = 3.5$. Taking half-integer values of m like this will maximally violate the loop closure condition. The resulting fidelity for this mapping is therefore significantly lower than before, at 0.9161.

We see from Figures 4 and 5 that the impact of the MS unitary on the motional state will be in part to cause sinusoidal oscillations in the expectation of the phonon occupation number, where the number of oscillations is given by the loop closure parameter m . We introduce in the following a more powerful tool to visualise the phonon state trajectories, namely, we will analyse instead the trajectories of these states in phase-space.

The motivation for this analysis can be found in Section 6.4, where the impact of this motion in the presence of motional heating is discussed. Although loop closure implies that its contribution can be eliminated at the gate time, noise sources affecting the phonon subspace can still lead to a reduction in fidelity as a result of the coupling with the qubit subspace *during* the gate's execution. Thus we cannot entirely disregard this term. Further, a thorough understanding of the phonon dynamics in phase-space gives a useful way to visualise loop closure geometrically. This becomes useful when considering other architectures that may utilise different phonon trajectories for speed or error mitigation (for example, as seen in [10] and [15]).

We begin by restating here the full form of the evolution operator $U(t)$ given in (30):

$$U(t) = \exp\left(\frac{\eta\Omega_R}{2\delta}\hat{S}_y^{(\phi)}((e^{i\delta t} - 1)\hat{a} - (e^{-i\delta t} - 1)\hat{a}^\dagger)\right) \cdot \exp\left(-i\left(\frac{\eta\Omega_R}{2\delta}\right)^2\hat{S}_y^{(\phi)2}(\delta t - \sin(\delta t))\right) \quad (40)$$

In the language of quantum optics [14], we will refer to the first term in the unitary as the *displacement operator* $\hat{D}(\alpha\hat{S}_y^{(\phi)})$, defined by $\hat{D}(\beta) \equiv \exp(\beta\hat{a}^\dagger - \beta^*\hat{a})$. For consistency with this form, we have taken $\alpha(t) = \frac{\eta\Omega_R}{2\delta}(1 - e^{-i\delta t})$. A derivation of some of the key properties of this operator is provided in Appendix A.2. Crucially, we find there that $\hat{D}(\beta)$ has the effect of displacing the phase-space coordinates of the motional state of the phonons by the vector $\beta \in \mathbb{C}$. More specifically, for the displacement by $\alpha(t)$ defined as above, we expect to obtain trajectories of expectation values displaced by $\text{Re}(\alpha(t)) = \frac{\eta\Omega_R}{2\delta}(1 - \cos(\delta t))$ in position and by $\text{Im}(\alpha(t)) = \frac{\eta\Omega_R}{2\delta}\sin(\delta t)$ in momentum. This gives us a circle of radius $\frac{\eta\Omega_R}{2\delta}$ in phase-space, traversed in the clockwise direction.

To complete the displacement operator equivalency, it will be necessary to separate out the $\hat{S}_y^{(\phi)}$ term in the argument of $\hat{D}(\alpha\hat{S}_y^{(\phi)})$ [6][7]. This can be achieved by diagonalisation of $\hat{S}_y^{(\phi)} = \sum_j \lambda_j |j\rangle\langle j|$ to obtain:

$$\begin{aligned} \hat{D}(\alpha\hat{S}_y^{(\phi)}) &= \exp((\alpha\hat{a}^\dagger - \alpha^*\hat{a})\hat{S}_y^{(\phi)}) \\ &= \sum_j \exp((\alpha\hat{a}^\dagger - \alpha^*\hat{a})\lambda_j) |j\rangle\langle j| \\ &= \sum_j \hat{D}(\alpha\lambda_j) |j\rangle\langle j| \end{aligned} \quad (41)$$

Noting that $\hat{S}_y^{(\phi)} \equiv \hat{\sigma}_y^{(\phi)} \otimes \mathbb{I} + \mathbb{I} \otimes \hat{\sigma}_y^{(\phi)}$, where the Pauli matrix $\hat{\sigma}_y^{(\phi)}$ has eigenvalues 1 and -1 , this immediately gives us possible values of $\lambda_j = 0, 0, 2, -2$. Substituting into (41), we obtain:

$$\hat{D}(\alpha\hat{S}_y^{(\phi)}) = \hat{D}(2\alpha)\hat{P}_2 + \hat{D}(-2\alpha)\hat{P}_{-2} + \hat{P}_0, \quad (42)$$

where \hat{P}_λ denotes the projector mapping the electronic qubit space onto the subspace with eigenvalue λ for $\hat{S}_y^{(\phi)}$. The expression given in (42) motivates the interpretation of $\hat{D}(\alpha\hat{S}_y^{(\phi)})$ as a 'state-dependent' displacement operator [7], as we see that it will have the effect of inducing displacements in phase-space to the motional state by an amount *conditional* on the internal electronic states of the ions.

Figure 6 shows the trajectories of the motional states in phase-space obtained for different initial Fock states $|n\rangle$. The plots are obtained by taking the expectation values of rescaled position and momentum operators $\hat{X}_1 \equiv \frac{1}{2}(\hat{a} + \hat{a}^\dagger)$ and $\hat{X}_2 \equiv \frac{1}{2i}(\hat{a} - \hat{a}^\dagger)$ respectively. In order that we isolate the behaviour of the displacement operator, the second entangling term in (40) is eliminated by transforming to a frame rotating with this term. Further, (42) tells us that in order to observe pure displacement mappings, it will be necessary to project the qubit state onto one of the projection subspaces of \hat{P}_2 or \hat{P}_{-2} before taking expectation values. For the plots obtained in Figure 6, the $\lambda = 2$ subspace is chosen arbitrarily. Importantly, we observe that all trajectories form identical closed loops in phase-space, as required, which is consistent with the requirement of loop closure irrespective of motional state. For a detailed justification of how this arises mathematically, the reader is again referred to Appendix A.2.

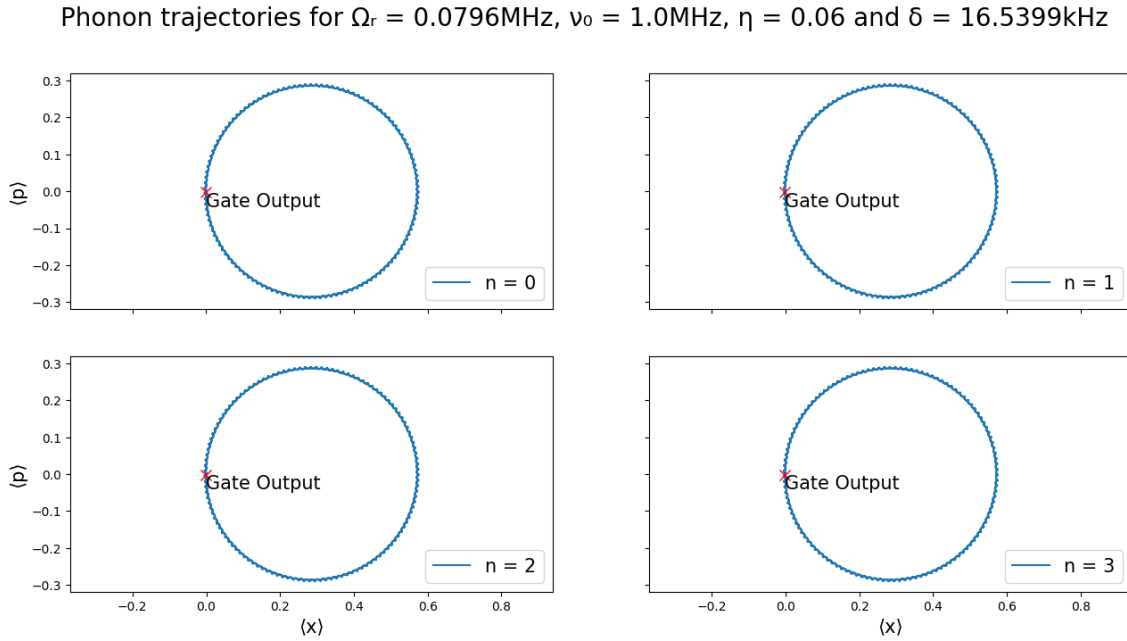


Figure 6: Phase-space trajectories of the motional states of the ions. The trajectories are plotted for initial Fock states $|n\rangle$ for $n = 0, 1, 2, 3$, and we see that they are all identical. The detuning δ is chosen in accordance with (39) with an integer value of $m = 3$. This means that for each case, 3 laps of the loops shown are completed by the gate time. We have taken the input qubit state to equal $\frac{1}{2}(|g\rangle + |e\rangle) \otimes (|g\rangle + |e\rangle)$, or equivalently, the projection state of the \hat{P}_2 projector, such that from (42) we expect pure displacements by $2\alpha(t)$. For the \hat{P}_{-2} subspace, the trajectories would look identical, still beginning and ending at the origin, but will be reflected in the x -axis. For the \hat{P}_0 subspace, the motional states experience no displacement. The plots are obtained using a Lindblad master equation solver as with Figures 4 and 5, again with the full Hamiltonian given in (15). The bumps in the circular trajectory giving a flower-like pattern correspond to excitations of the far off-resonant sidebands, which we did not consider in the simplified Hamiltonian given in (22) used to derive the evolution unitary in (30).

5 Impact of Carrier Transition

This section provides a rough, non-rigorous overview of the low-order impacts of the carrier transition in limiting the MS gate fidelity. Modelling the gate effectively in the presence of these off-resonant effects is far from trivial, as the most straightforward approach of calculating a complete Magnus expansion becomes far more cumbersome to calculate at low order, and near intractable at higher

orders. Thus, the approach demonstrated here serves only to give insight into the dominant effects of the carrier transition, and disregards higher order terms that can be safely neglected when we only slightly push beyond the weak-driving regime.

Firstly, to motivate why it becomes necessary to consider the carrier transition at all, we consider what happens when we attempt to speed up the gate. This is of critical importance, as slow gate speeds are one of the most pressing challenges faced by trapped-ion quantum computing. Although this modality boasts unrivaled coherence times and record fidelities, when comparing to competing modalities such as superconducting qubits, the gate speeds for 2-qubit entangling unitaries are typically several orders of magnitude lower [4].

To decrease the gate time, the most obvious approach would be to increase the effective Rabi frequency $\frac{\Omega_R^2 \eta^2}{2\delta}$, which experimentally is typically achieved by increasing Ω_R . The Lamb-Dicke factor η is less experimentally accessible as a variable parameter, and the detuning δ was formerly shown to be proportional to Ω_R by consequence of loop closure. Thus, the solution would be to increase Ω_R , which is typically achieved by increasing the laser amplitude E_0 .

In the following we will show that increasing Ω_R relative to the carrier detuning $\nu_0 + \delta$ will increase the effects of the carrier transition, thus forcing us to consider its effects when constructing faster gates. The procedure we use here is *adiabatic elimination*, where we start from the complete Schrodinger equation involving all relevant states and couplings, then assuming that some probability amplitudes will evolve much faster than others, we can *adiabatically eliminate* the off-resonant states and obtain an effective system of equations for the dynamics of the resulting two-level system. Although this is a less rigorous method than the Dyson series or Magnus expansion, it is far simpler to calculate and still recovers the core features of the carrier effects at low order.

5.1 Adiabatic Elimination of Carrier Transition Levels

We begin by restating (18) here to give the form of the Hamiltonian for the trapped-ion system prior to making the second RWA:

$$\begin{aligned}\tilde{H}_{int} &= \sum_{j=1}^{\#ions} \frac{\hbar\Omega_R}{2} (e^{i((\nu_0+\delta)t+\phi)} + e^{i((- \nu_0-\delta)t+\phi)}) \hat{\sigma}_+^{(j)} + h.c. \\ &\quad + \frac{i\hbar\eta\Omega_R}{2} (e^{i(\delta t+\phi)} + e^{i((-2\nu_0-\delta)t+\phi)}) \hat{\sigma}_+^{(j)} \hat{a} + h.c. \\ &\quad + \frac{i\hbar\eta\Omega_R}{2} (e^{i((2\nu_0+\delta)t+\phi)} + e^{i(-\delta t+\phi)}) \hat{\sigma}_+^{(j)} \hat{a}^\dagger + h.c. \\ &= \frac{\hbar\Omega_R}{2} \hat{S}_+ (e^{i((\nu_0+\delta)t+\phi)} + e^{i((- \nu_0-\delta)t+\phi)}) + h.c. + \text{sideband terms}.\end{aligned}\tag{43}$$

We immediately take $\phi = \frac{\pi}{2}$ for ease of calculation, as we know from Section 3 that this choice recovers the correct MS unitary in the absence of the carrier transition. We also define $\Delta \equiv \delta + \nu_0$ for ease of notation. This yields:

$$\tilde{H}_{int} = \frac{i\hbar\Omega_R}{2} \hat{S}_+ (e^{i\Delta t} + e^{-i\Delta t}) + h.c. + \text{sideband terms}.\tag{44}$$

For now we only care about the transition $|gg\rangle \leftrightarrow |ee\rangle$. We will work in the reduced basis of $\{|gg, n\rangle, |ge, n\rangle, |eg, n\rangle, |ee, n\rangle\}$ such that we only consider the carrier transition effects (the sideband

terms for the core MS interaction will be added in later). The goal will be to obtain and solve differential equations for the probability amplitudes c_{ggn} and c_{een} defined by the Schrodinger equation:

$$i\frac{d}{dt}\vec{c} = \frac{1}{\hbar}\tilde{H}_{int}\vec{c} \quad (45)$$

The relevant matrix elements will therefore be given by:

$$\langle eg, n | \tilde{H}_{int} | gg, n \rangle, \langle ge, n | \tilde{H}_{int} | gg, n \rangle, \langle ee, n | \tilde{H}_{int} | ge, n \rangle, \langle ee, n | \tilde{H}_{int} | eg, n \rangle \quad (46)$$

By considering the form of the Hamiltonian, we see that these will all be equivalent, given by:

$$\frac{i\hbar\Omega_R}{2}(e^{i\Delta t} + e^{-i\Delta t}) = i\hbar\Omega_R\cos(\Delta t) \quad (47)$$

In order to solve for c_{ggn} and c_{een} in the presence of the carrier transition, we will first require the time evolution of amplitudes c_{gen} and c_{egn} in terms of c_{ggn} and c_{een} . Substituting in the matrix elements obtained in (47) to the corresponding Schrodinger equations for these states (where we assume that all states other than $|gg, n\rangle$ and $|ee, n\rangle$ are never meaningfully populated), we obtain:

$$\frac{d}{dt}c_{gen} = \frac{d}{dt}c_{egn} = \Omega_R\cos(\Delta t)(c_{ggn} - c_{een}) \quad (48)$$

Thus, $c_{gen}(t)$ and $c_{egn}(t)$ can be obtained by integrating (48):

$$c_{gen}(t) - c_{gen}(0) = c_{egn}(t) - c_{egn}(0) = \Omega_R \int_0^t dt' \cos(\Delta t')(c_{ggn}(t') - c_{een}(t')) \quad (49)$$

To obtain the particular mapping for input $|ee, n\rangle$, we take the states $|ge, n\rangle$ and $|eg, n\rangle$ to be initially unpopulated. Thus, we can set $c_{gen}(0) = c_{egn}(0) = 0$.

We now take the adiabatic limit, where Δ is assumed to be much larger than the effective Rabi frequency Ω for the MS gate oscillations. In this limit, we assume that $c_{ggn}(t)$ and $c_{een}(t)$ will remain roughly constant within one cycle of oscillations at the fast frequency Δ , as the timescale of the MS gate dynamics is much slower at frequency Ω . To first order, within the k^{th} cycle at frequency Δ :

$$c_{ggn}(t) \approx c_{ggn}(t_k) + (t - t_k)\dot{c}_{ggn}(t_k) \quad (50)$$

We divide the integral in (49) into a sum of smaller integrals over each full oscillation at the fast frequency Δ , then add the residual term leftover at the end after the final complete cycle. Defining T_k to be the time at the end of the last complete oscillation at frequency Δ , we obtain:

$$\begin{aligned} c_{gen}(t) = & \sum_{k=0}^{\text{\#full cycles}-1} \Omega_R \int_{t_k}^{t_k + \frac{2\pi}{\Delta}} dt' \cos(\Delta t')(c_{ggn}(t') - c_{een}(t')) \\ & + \Omega_R \int_{T_k}^t dt' \cos(\Delta t')(c_{ggn}(t') - c_{een}(t')) \end{aligned} \quad (51)$$

First we consider the sum over complete cycles. Substituting in (50), we obtain:

$$\begin{aligned}
c_{gen}(T_k) &= \Omega_R \sum_k \int_{t_k}^{t_k + \frac{2\pi}{\Delta}} \cos(\Delta t') (c_{ggn}(t_k) + (t - t_k) \dot{c}_{ggn}(t_k) - c_{een}(t_k) - (t - t_k) \dot{c}_{een}(t_k)) dt' \\
&= \Omega_R \sum_k \int_0^{\frac{2\pi}{\Delta}} t' \cos(\Delta t') (\dot{c}_{ggn}(t_k) - \dot{c}_{een}(t_k)) dt'
\end{aligned} \tag{52}$$

Integrating by parts, we find that this contribution at first order will vanish exactly. This is a consequence of the symmetry of the detuning from the two sidebands. The physical interpretation of this cancellation is that there will be no leading order AC Stark shift due to the carrier transition [6][7]. We therefore need to expand to second order:

$$\begin{aligned}
c_{gen}(T_k) &= \Omega_R \sum_k \int_{t_k}^{t_k + \frac{2\pi}{\Delta}} \cos(\Delta t') \left(\frac{1}{2} (t - t_k)^2 \ddot{c}_{ggn}(t_k) - \frac{1}{2} (t - t_k)^2 \ddot{c}_{een}(t_k) \right) dt' \\
&= \frac{\Omega_R}{2} \sum_k \int_0^{\frac{2\pi}{\Delta}} t'^2 \cos(\Delta t') (\ddot{c}_{ggn}(t_k) - \ddot{c}_{een}(t_k)) dt' \\
&= \frac{\Omega_R}{2} \sum_k \frac{4\pi}{\Delta^3} (\ddot{c}_{ggn}(t_k) - \ddot{c}_{een}(t_k))
\end{aligned} \tag{53}$$

In the limit of small $\frac{4\pi}{\Delta}$ relative to the timescale of variation in $c_{ggn}(t)$ and $c_{een}(t)$, this sum tends to an integral:

$$\begin{aligned}
c_{gen}(T_k) &= \frac{\Omega_R}{2} \sum_k \frac{4\pi}{\Delta^3} (\ddot{c}_{ggn}(t_k) - \ddot{c}_{een}(t_k)) \\
&\rightarrow \frac{\Omega_R}{2} \cdot \frac{2}{\Delta^2} \int_0^{T_k} dt' (\ddot{c}_{ggn}(t') - \ddot{c}_{een}(t')) \\
&= \frac{\Omega_R}{\Delta^2} (\dot{c}_{ggn}(T_k) - \dot{c}_{een}(T_k))
\end{aligned} \tag{54}$$

We now account for the residual part after all complete cycles. For consistency with above, we again expand to second order:

$$\begin{aligned}
c_{gen}(t) - c_{gen}(T_k) &= \Omega_R \int_{T_k}^t dt' \cos(\Delta t') (c_{ggn}(t') - c_{een}(t')) \\
&= \Omega_R \int_0^{t'-T_k} \cos(\Delta t') (c_{ggn}(T_k) - c_{een}(T_k)) dt' \\
&\quad + \Omega_R \int_0^{t'-T_k} t' \cos(\Delta t') (\dot{c}_{ggn}(T_k) - \dot{c}_{een}(T_k)) dt' \\
&\quad + \frac{\Omega_R}{2} \int_0^{t'-T_k} t'^2 \cos(\Delta t') (\ddot{c}_{ggn}(T_k) - \ddot{c}_{een}(T_k)) dt' \\
&= \Omega_R (c_{ggn}(T_k) - c_{een}(T_k)) \frac{\sin(\Delta t)}{\Delta} \\
&\quad + \Omega_R (\dot{c}_{ggn}(T_k) - \dot{c}_{een}(T_k)) \left(\frac{t - T_k}{\Delta} \sin(\Delta t) + \frac{1}{\Delta^2} \cos(\Delta t) - \frac{1}{\Delta^2} \right) \\
&\quad + \frac{\Omega_R}{2} (\ddot{c}_{ggn}(T_k) - \ddot{c}_{een}(T_k)) \left(\frac{(t - T_k)^2}{\Delta} \sin(\Delta t) + \frac{2(t - T_k)}{\Delta^2} \cos(\Delta t) - \frac{2}{\Delta^3} \sin(\Delta t) \right)
\end{aligned} \tag{55}$$

Adding this to the result of (54), we obtain:

$$\begin{aligned}
c_{gen}(t) &= \Omega_R (c_{ggn}(T_k) - c_{een}(T_k)) \frac{\sin(\Delta t)}{\Delta} \\
&\quad + \Omega_R (\dot{c}_{ggn}(T_k) - \dot{c}_{een}(T_k)) \left(\frac{t - T_k}{\Delta} \sin(\Delta t) + \frac{1}{\Delta^2} \cos(\Delta t) - \frac{1}{\Delta^2} + \frac{1}{\Delta^2} \right) \\
&\quad + \frac{\Omega_R}{2} (\ddot{c}_{ggn}(T_k) - \ddot{c}_{een}(T_k)) \left(\frac{(t - T_k)^2}{\Delta} \sin(\Delta t) + \frac{2(t - T_k)}{\Delta^2} \cos(\Delta t) - \frac{2}{\Delta^3} \sin(\Delta t) \right) \\
&= \frac{\Omega_R}{\Delta} \sin(\Delta t) (c_{ggn}(T_k) + (t - T_k) \dot{c}_{ggn}(T_k) + \frac{1}{2} (t - T_k)^2 \ddot{c}_{ggn}(T_k) + \dots) \\
&\quad - \frac{\Omega_R}{\Delta} \sin(\Delta t) (c_{een}(T_k) + (t - T_k) \dot{c}_{een}(T_k) + \frac{1}{2} (t - T_k)^2 \ddot{c}_{een}(T_k) + \dots) \\
&\quad + \frac{\Omega_R}{\Delta^2} \cos(\Delta t) ((\dot{c}_{ggn}(T_k) - \dot{c}_{een}(T_k)) + (t - T_k) (\ddot{c}_{ggn}(T_k) - \ddot{c}_{een}(T_k)) + \dots) \\
&\quad + O\left(\frac{\Omega_R}{\Delta^3}\right) \\
&= \frac{\Omega_R}{\Delta} \sin(\Delta t) (c_{ggn}(t) - c_{een}(t)) + \frac{\Omega_R}{\Delta^2} \cos(\Delta t) (\dot{c}_{ggn}(t) - \dot{c}_{een}(t)) + \dots
\end{aligned} \tag{56}$$

Thus, we obtain a leading order expression for $c_{gen}(t)$ (and the equivalent result for $c_{egn}(t)$) in terms of $c_{ggn}(t)$ and $c_{een}(t)$. Substituting these into the Schrodinger equations for $c_{ggn}(t)$ and $c_{een}(t)$ allows us to obtain a set of coupled linear differential equations for this subspace. For a more rigorous analysis, we will also require the full matrix element contributions from the sideband terms containing $c_{ge,n\pm 1}$ and $c_{eg,n\pm 1}$, however, for simplicity, we assume that the MS interaction generated by the sideband transitions can be well-approximated by simple Rabi oscillations at the previously defined effective Rabi frequency Ω . Thus, for the purposes of finding the leading order effects of the carrier transition, we neglect the motion of the phonon states in phase space, and the additional $-\sin(\delta t)$ term in the propagator for the entangling MS interaction. This result will be equivalent to adiabatically eliminating the amplitudes $c_{ge,n\pm 1}$ and $c_{eg,n\pm 1}$ by taking them to be sufficiently off-resonant that they are never meaningfully populated. Thus, ignoring the carrier terms for now, the dynamics we obtain from the MS interaction will approximately be given by:

$$\begin{cases} i\dot{c}_{een} = \Omega(c_{ggn} + c_{een}) \\ i\dot{c}_{ggn} = \Omega(c_{ggn} + c_{een}) \end{cases} \quad (57)$$

Now accounting for the carrier terms:

$$\begin{cases} i\dot{c}_{een} = \Omega(c_{ggn} + c_{een}) + i\hbar\Omega_R\cos(\Delta t)(c_{egn} + c_{gen}) \\ i\dot{c}_{ggn} = \Omega(c_{ggn} + c_{een}) - i\hbar\Omega_R\cos(\Delta t)(c_{egn} + c_{gen}) \end{cases} \quad (58)$$

Substituting in the results of (56), we obtain:

$$\begin{cases} i\dot{c}_{een} = \Omega(c_{ggn} + c_{een}) + \frac{i\Omega_R^2}{\Delta^2}\sin(2\Delta t)(c_{ggn} - c_{een}) + \frac{2i\Omega_R^2}{\Delta^2}\cos^2(\Delta t)(\dot{c}_{ggn} - \dot{c}_{een}) \\ i\dot{c}_{ggn} = \Omega(c_{ggn} + c_{een}) - \frac{i\Omega_R^2}{\Delta^2}\sin(2\Delta t)(c_{ggn} - c_{een}) - \frac{2i\Omega_R^2}{\Delta^2}\cos^2(\Delta t)(\dot{c}_{ggn} - \dot{c}_{een}) \end{cases} \quad (59)$$

For ease of notation, we define $f(t) \equiv \frac{2\Omega_R^2}{\Delta^2}\cos^2(\Delta t)$ and $g(t) \equiv i\frac{\Omega_R^2}{\Delta}\sin(2\Delta t)$. Expressing (59) in matrix form:

$$\begin{aligned} i\dot{\vec{c}} &= \Omega \begin{pmatrix} 1 & 1 \\ 1 & 1 \end{pmatrix} + g(t) \begin{pmatrix} 1 & -1 \\ -1 & 1 \end{pmatrix} \vec{c} + if(t) \begin{pmatrix} 1 & -1 \\ -1 & 1 \end{pmatrix} \dot{\vec{c}} \\ \Rightarrow i \begin{pmatrix} 1-f(t) & f(t) \\ f(t) & 1-f(t) \end{pmatrix} \dot{\vec{c}} &= \begin{pmatrix} \Omega+g(t) & \Omega-g(t) \\ \Omega-g(t) & \Omega+g(t) \end{pmatrix} \vec{c} \end{aligned} \quad (60)$$

By observation, the basis $\{|\pm\rangle\}$ (defined here by $|\pm\rangle \equiv \frac{|ee\rangle \pm |gg\rangle}{\sqrt{2}}$) will diagonalise this system. Re-expressing the matrices in this basis, we obtain:

$$i \begin{pmatrix} 1 & 0 \\ 0 & 1-2f(t) \end{pmatrix} \dot{\vec{c}} = \begin{pmatrix} 2\Omega & 0 \\ 0 & 2g(t) \end{pmatrix} \vec{c} \quad (61)$$

Solving this decoupled system yields:

$$c_+(t) = c_+(0)\exp(-2i\Omega t) \quad (62)$$

$$c_-(t) = c_-(0)\sqrt{\frac{1-4\alpha\cos^2(\Delta t)}{1-4\alpha}}, \quad (63)$$

where $\alpha = \frac{\Omega_R^2}{\Delta^2}$. Expanding for small α :

$$\begin{aligned} c_-(t) &= c_-(0)(1-2\alpha\cos^2(\Delta t))(1+2\alpha) \\ &= c_-(0)(1+2\alpha\sin^2(\Delta t)) + O(\alpha^2) \end{aligned} \quad (64)$$

Thus, taking the particular input of $c_{een}(0) = 1$, we can take the initial conditions $c_+ = c_- = \frac{1}{\sqrt{2}}$. Lastly, we can now combine the results of $c_+(t)$ and $c_-(t)$ to obtain the dynamics of $c_{een}(t)$:

$$\begin{aligned}
c_{een}(t) &= \frac{1}{\sqrt{2}}(c_+(t) + c_-(t)) \\
&= \frac{1}{2}(e^{-2i\Omega t} + 1 + 2\alpha \sin^2(\Delta t)) \\
&= \frac{e^{-i\Omega t}}{2}(e^{-i\Omega t} + e^{i\Omega t} + 2\alpha e^{i\Omega t} \sin^2(\Delta t)) \\
&= e^{-i\Omega t}(\cos(\Omega t) + \alpha e^{i\Omega t} \sin^2(\Delta t))
\end{aligned} \tag{65}$$

And similarly, for $c_{ggn}(t)$:

$$\begin{aligned}
c_{ggn}(t) &= \frac{1}{\sqrt{2}}(c_+(t) - c_-(t)) \\
&= e^{-i\Omega t}(-i\sin(\Omega t) - \alpha e^{i\Omega t} \sin^2(\Delta t))
\end{aligned} \tag{66}$$

Thus, ignoring the global phase, we again obtain Rabi oscillations at frequency Ω giving the familiar MS gate mappings at $\Omega t = \frac{\pi}{4}$. However, this becomes superposed by fast oscillations at frequency Δ and with amplitude $\alpha = \frac{\Omega_R^2}{\Delta^2}$. This justifies the prior claim that as we increase the Rabi frequency relative to the carrier detuning, the effects of the carrier transition become more dominant in the dynamics of the system, and in particular we find that these effects will scale quadratically with this ratio.

5.2 Verification of Carrier Transition Effects

To test the validity of the result obtained in (65) and (66), we consider how the fidelity of the gate changes as Ω_R is varied such that Δt is chosen to be an integer or half-integer multiple of π . We expect that for integer multiples of π , the carrier effects should be eliminated up to order α , whereas for the half-integer case, we should expect the gate infidelity to increase quadratically with $\frac{\Omega_R}{\Delta}$ (assuming loop closure and other conditions listed at the start of Section 4 are met). Although experimentally, this level of precision is typically not attainable, arbitrary precision is possible within a numerical simulation, thus we test this prediction using a Lindblad master equation solver run on the Hamiltonian given in (18). Figure 7 shows the results obtained for the integer and half-integer cases. Figure 8 shows visible fast oscillations at frequency Δ in the expectation value of $|ee\rangle\langle ee| - |gg\rangle\langle gg|$.

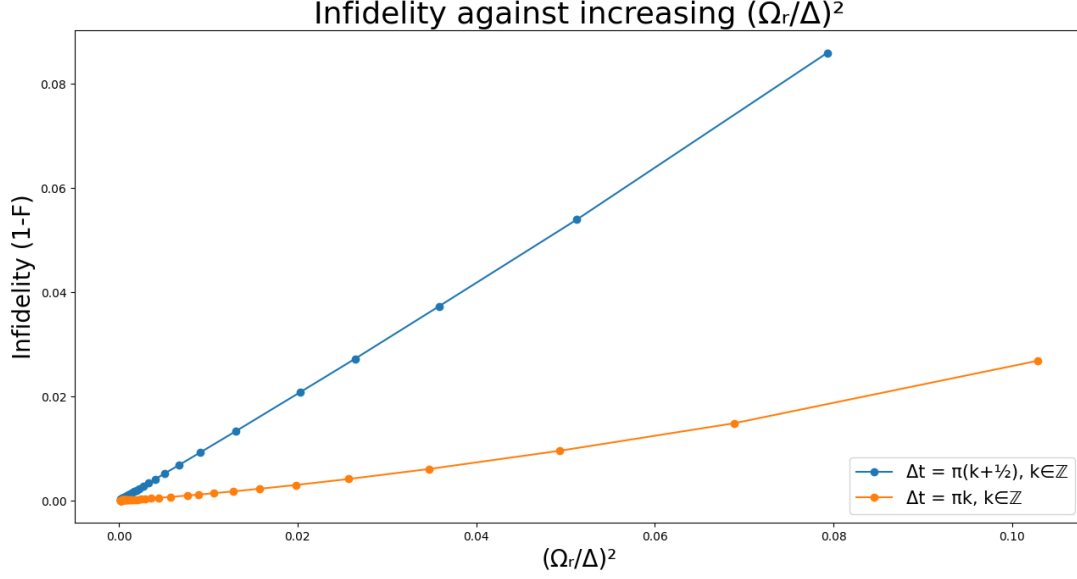


Figure 7: The infidelities for the mappings of $|gg\rangle$ to $\frac{1}{\sqrt{2}}(|gg\rangle - i|ee\rangle)$ are seen to increase linearly with $(\frac{\Omega_R}{\Delta})^2$ when $\Delta t_g = (k + \frac{1}{2})\pi, k \in \mathbb{Z}$. This is consistent with what we expect from (65,66). However, contrary to the predictions of (65,66), we also see a smaller but non-negligible rise in the infidelity for integer multiples of π . This can partly be explained by excitations of the off-resonant sidebands, where the red detuned laser excites the blue sideband and vice versa to a non-negligible degree. These will be the next most dominant effects to consider, being smaller only by a factor of η . Further, for larger Ω_R , we also expect terms of order $(\frac{\Omega_R}{\Delta})^4$ to begin to contribute to the dynamics, which already become non-negligible at ~ 0.01 for $\frac{\Omega_R}{\Delta} \sim 0.1$.

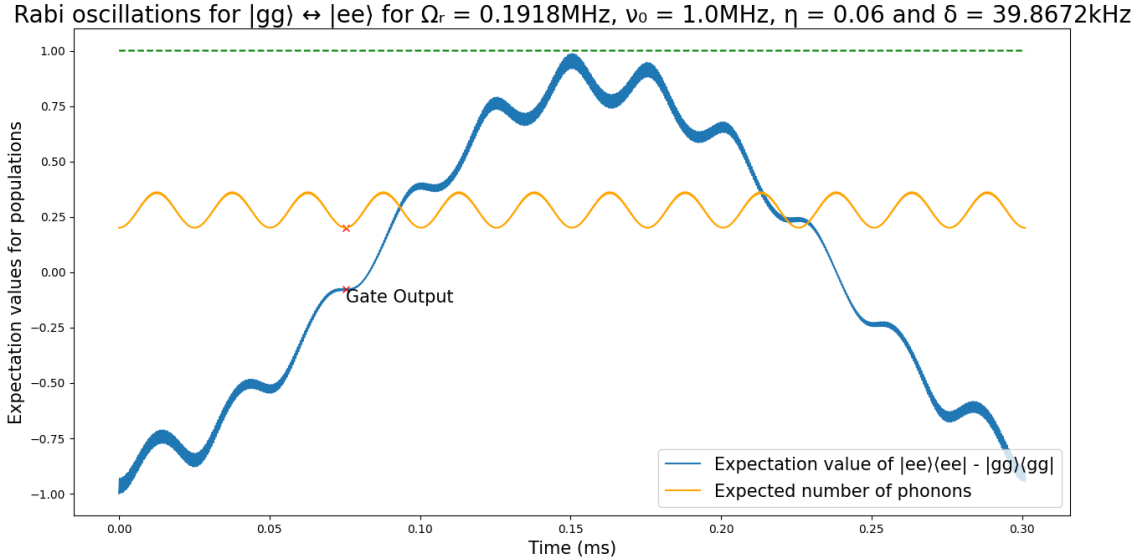


Figure 8: Off-resonant Rabi oscillations at frequency Δ visible for larger Ω_R . We observe that the amplitude of these oscillations appears modulated with the slow oscillations at frequency Ω , such that they are largest for $\Omega t = 0, \frac{\pi}{2}, \pi$, and are smaller at the gate output time. This is due to the variation of the phase of these oscillations with Ωt , as predicted by (65,66). Note this plot also shows fast oscillations due to the far off-resonant sideband transitions which are superposed onto the carrier oscillations, which explains why the visible oscillations are reduced, but do not completely vanish at the gate time.

6 Other noise sources

Thus far, we have focused largely on error sources that are inherent to the original Hamiltonian stated in (9). These have arisen by virtue of the fundamental dynamics of the laser-ion interaction not giving exactly the MS gate we want to construct. These errors include (but are not limited to) [3]:

- Higher order terms in the Lamb-Dicke expansion of $O(\eta^2)$.
- Off-resonant phonon modes beyond just the centre-of-mass mode considered here. In the literature, these are often referred to as 'spectator modes' [3].
- Off-resonant excitations of transitions such as the carrier and far off-resonant sidebands. These may induce unwanted fast oscillations (as seen in Section 5) and AC Stark shifts.
- Errors resulting from imperfect tuning of pulse lengths, detunings, laser amplitudes and phase.

In this section, we will focus instead on external error sources that have not already been accounted for in the Hamiltonian. The effects we will analyse here are given by the following (note this is again not an exhaustive list, but it is sufficiently broad for giving insight into the key noise mechanisms for trapped-ion qubits):

- Spontaneous emission between the electronic logical qubit levels. In the case of hyperfine or Zeeman qubits, where the logical states may be connected via Raman transitions, spontaneous emission from this Raman virtual level will need to be considered instead. However, we restrict our analysis here to the case of directly driven transitions.
- Dephasing due to stray electric and magnetic field noise.
- Heating of the motional phonon modes due to electric field noise.

For each of the above processes, we will derive physically their impacts on the system using the formalism of quantum noise and quantum operations. A more in depth discussion of the theory of open systems is provided in [1] and [12], but a short summary of the key results is provided in the following. We will then use this formalism to describe and analyse the dynamics resulting from each of the above effects.

6.1 Dynamics of open systems

We provide here a short overview of two useful mathematical tools for describing the dynamics of open quantum systems. The first will be the *operator-sum representation* for quantum operations [1][12]. This is a useful formalism for analysing the dynamics of a system weakly coupled to its environment, without needing to model the entire joint system including the environment Hilbert space. Thus it becomes a very useful tool for describing and understanding the effects of noise in quantum channels. The second will be the *Lindblad master equation* [12], and we will treat it here as an extension of the quantum operation formalism to allow us to further describe the dynamics of open systems as a first-order differential equation, much like the Schrodinger and von Neumann equations for closed systems, in order to allow us to obtain their continuous time evolution.

Consider some system S with state given by the density matrix ρ_S . We are interested in finding the dynamics of ρ_S , which in the absence of any noise, we know will be governed by the von Neumann equation $\frac{d}{dt}\rho = -\frac{i}{\hbar}[H, \rho]$, where H is the Hamiltonian for the space S . However, suppose now that the space S is weakly coupled to its environment, described also by some Hilbert space which we will denote E . We now will instead be dealing with the joint system $S \otimes E$, which in general will undergo

some unitary evolution $U_{tot}(t)$ due to the overall Hamiltonian of the joint system. We still want to find the dynamics just of ρ_S , which we obtain by taking a partial trace over the environment space:

$$\rho_S(t) = \text{tr}_{env}(U_{tot}\rho_{(S\otimes E)}U_{tot}^\dagger) \quad (67)$$

The presence of interactions with the environment has important consequences for the dynamics of ρ_S , most notably that it need not necessarily be strictly unitary anymore. We will show here that the resulting dynamics can be represented in what is called the *operator-sum* or *Kraus* representation for quantum operations. To obtain this, we first make two simplifying assumptions about the joint system. Firstly, the initial state of $\rho_{(S\otimes E)}$ is assumed to be a product state $\rho_S(0) \otimes \rho_E(0)$. This assumption will be valid for quantum computing setups where initial states of the system are prepared and correlations with the environment are destroyed at $t = 0$ [1]. Secondly, the environment state is assumed to be initially some pure state $|e_0\rangle$, rather than a general mixed state. This requirement can always be satisfied by expanding the environment space E and 'purifying' the density matrix into a pure state [1]. Taking these two assumptions to be met, we define the basis $\{|e_k\rangle\}$ to span the environment space E in order to take the partial trace, and can obtain the dynamics for ρ_S in the following [1][12]:

$$\begin{aligned} \rho_S(t) &= \text{tr}_{env}(U_{tot}(\rho_S \otimes |e_0\rangle\langle e_0|)U_{tot}^\dagger) \\ &= \sum_k \langle e_k|U_{tot}(\rho_S \otimes |e_0\rangle\langle e_0|)U_{tot}^\dagger|e_k\rangle \\ &= \sum_k E_k \rho_S E_k^\dagger, \end{aligned} \quad (68)$$

where $E_k \equiv \langle e_k|U_{tot}|e_0\rangle$ are operators that by construction will only act on the system space S . These operators are called *operation elements* or *Kraus operators*, and the summation of the result of acting on ρ_S with these operators gives the *operator-sum representation* for describing the resulting quantum operation on ρ_S .

We now consider the *Lindblad master equation* [1][12], given by:

$$\frac{d}{dt}\rho_S = -\frac{i}{\hbar}[H, \rho_S] + \sum_j \hat{L}_j \rho_S \hat{L}_j^\dagger - \frac{1}{2}\{\hat{L}_j^\dagger \hat{L}_j, \rho_S\}, \quad (69)$$

where $\{A, B\}$ denotes the anticommutator $AB + BA$. This provides a complementary picture to the operator-sum representation for describing open system dynamics, where the interaction between the system and environment is captured instead by the *Lindblad operators*, denoted by \hat{L}_j . Physically, we find that this picture is often more convenient to work with, as finding a complete set of time-dependent operation elements $E_k(t)$ quickly becomes non-trivial, especially when simultaneously accounting for evolution under H . Indeed all plots of gate dynamics in this paper (with and without noise) are obtained using a numerical Lindblad master equation solver.

One potential disadvantage of the master equation approach is that it is less general than the quantum operations formalism [1], as it relies on the assumption of Markovian dynamics for ρ_S , such that $\rho_S(t + dt)$ can be completely determined given $\rho_S(t)$ [12]. Fortunately, for many cases (including the noise processes we will consider here) this approximation is typically valid [12], and thus the Lindblad master equation becomes a powerful tool which we will use extensively in the following. A sketch of the derivation of (69) can be found in [12], where the strategy used there is to start from

an operator-sum representation for an arbitrary quantum operation mapping $\rho_S(0)$ to $\rho_S(dt)$, then comparing to a first-order Taylor expansion of $\rho_S(dt)$ about $\rho_S(0)$. The final form of the differential equation is obtained after comparing terms of order dt and invoking trace-preservation of ρ_S and the aforementioned requirement of Markovian dynamics.

6.2 Spontaneous Emission

We want to obtain operation elements E_k for spontaneous emission in order to obtain its operator-sum representation. To do this, we will need to consider the open system dynamics of each ion with the radiation field [9]. Up until this point we have adopted an entirely semi-classical picture, where the interaction Hamiltonian is assumed to take the form of an electric dipole perturbation $-\hat{d} \cdot \vec{E}$ for some electric dipole operator $\hat{d} \equiv -e\hat{r}$ and a classically well-defined electric field \vec{E} . This picture works well, as quantum properties of the radiation field become extremely well-approximated by the classical electromagnetic wave treatment for the strong coherent lasers that we deal with here. However, the semi-classical picture misses the phenomenon of *spontaneous emission*, which can only be described properly when we consider the coupling of the ion to the quantised radiation field [9]. The result of this is that we obtain non-zero matrix elements in the interaction Hamiltonian between multipole-connected electronic levels of the ion even in the absence of any photons, such that by Fermi's golden rule, the ion may *spontaneously* emit a photon and decay into the lower energy state without being driven by a laser [9]. A full QED treatment to recover this process is obviously overkill and wholly impractical, which motivates applying the quantum operations formalism as derived above for this process.

Let $|g, 0\rangle$ denote a state in the ground electronic state and with 0 photons (not phonons, these are not considered for the moment) in a particular mode with energy $\hbar\omega_0$ in the environment space. Even when allowing for spontaneous emission, this state will remain in this state indefinitely, as in the two-level picture we assume that there are no lower-energy multipole-connected states that it can decay to. However, in some time t , the excited state $|e, 0\rangle$ may spontaneously decay via emission of a photon to the state $|g, 1\rangle$ with some probability p , or remain in the state $|e, 0\rangle$ with probability $(1-p)$. Tracing over the environment, we therefore obtain for final photon states $|0\rangle$ and $|1\rangle$ respectively:

$$E_0 = \begin{pmatrix} 1 & 0 \\ 0 & \sqrt{1-p} \end{pmatrix}, \quad E_1 = \begin{pmatrix} 0 & \sqrt{p} \\ 0 & 0 \end{pmatrix} \quad (70)$$

The resulting quantum operation is known as *amplitude damping*. The operation element E_0 can be interpreted as leaving the state $|g\rangle$ unchanged, whilst reducing the amplitude of $|e\rangle$ by a factor of $\sqrt{1-p}$. The operation element E_1 can be interpreted as decaying the state $|e\rangle$ to $|g\rangle$, losing energy to the environment. Operating on ρ with these operation elements yields:

$$\begin{aligned} & \begin{pmatrix} 1 & 0 \\ 0 & \sqrt{1-p} \end{pmatrix} \begin{pmatrix} \rho_{00} & \rho_{01} \\ \rho_{10} & \rho_{11} \end{pmatrix} \begin{pmatrix} 1 & 0 \\ 0 & \sqrt{1-p} \end{pmatrix} + \begin{pmatrix} 0 & \sqrt{p} \\ 0 & 0 \end{pmatrix} \begin{pmatrix} \rho_{00} & \rho_{01} \\ \rho_{10} & \rho_{11} \end{pmatrix} \begin{pmatrix} 0 & 0 \\ \sqrt{p} & 0 \end{pmatrix} \\ &= \begin{pmatrix} \rho_{00} & \rho_{01}\sqrt{1-p} \\ \rho_{10}\sqrt{1-p} & \rho_{11}(1-p) \end{pmatrix} + \begin{pmatrix} \rho_{11}p & 0 \\ 0 & 0 \end{pmatrix} \\ &= \begin{pmatrix} \rho_{00} + \rho_{11}p & \rho_{01}\sqrt{1-p} \\ \rho_{10}\sqrt{1-p} & \rho_{11}(1-p) \end{pmatrix} \end{aligned} \quad (71)$$

Thus we obtain that the effect of spontaneous emission will be to map states towards the ground state $|g\rangle$ and to exponentially decay coherences between the $|g\rangle$ and $|e\rangle$ states. Note the trace of

the density matrix is necessarily preserved in this operation, ensuring that we still obtain a valid normalised density matrix after spontaneous emission.

We now reintroduce the bichromatic driving lasers to the system's dynamics in order to understand spontaneous emission within the context of the MS gate operation. Figure 9 demonstrates the results obtained for various decay rates in the regime where the frequency of the gate Rabi oscillations Ω is taken to be much faster than the rate of spontaneous emission γ (such that the ions do not all converge to the ground state). This regime is consistent with observed rates of spontaneous emission for real trapped-ion setups; for example, the decay time (defined by the time taken for the population of $|e\rangle$ to decay to $\frac{1}{e}$ of its initial value) for the excited level in the optical qubit used in the $^{40}\text{Ca}^+$ setup we considered in Section 4 was found to be 1.1 seconds, which is many orders of magnitude greater than typical gate times, which are of the order of microseconds [3][11]. For Zeeman and hyperfine qubits, the decay times are even longer, and are typically many orders of magnitude greater than any experimentally relevant timescales, such that its impact as a noise process becomes completely negligible [3]. Thus, we conclude that spontaneous emission is consequently far less significant than the other noise sources we will later consider, and is therefore typically not the most dominant experimental bottleneck for the construction of high fidelity gates.

Rabi oscillations for $|gg\rangle \leftrightarrow |ee\rangle$ for $\Omega_r = 0.0825\text{MHz}$, $\nu_0 = 1.0\text{MHz}$, $\eta = 0.06$ and $\delta = 17.1428\text{kHz}$

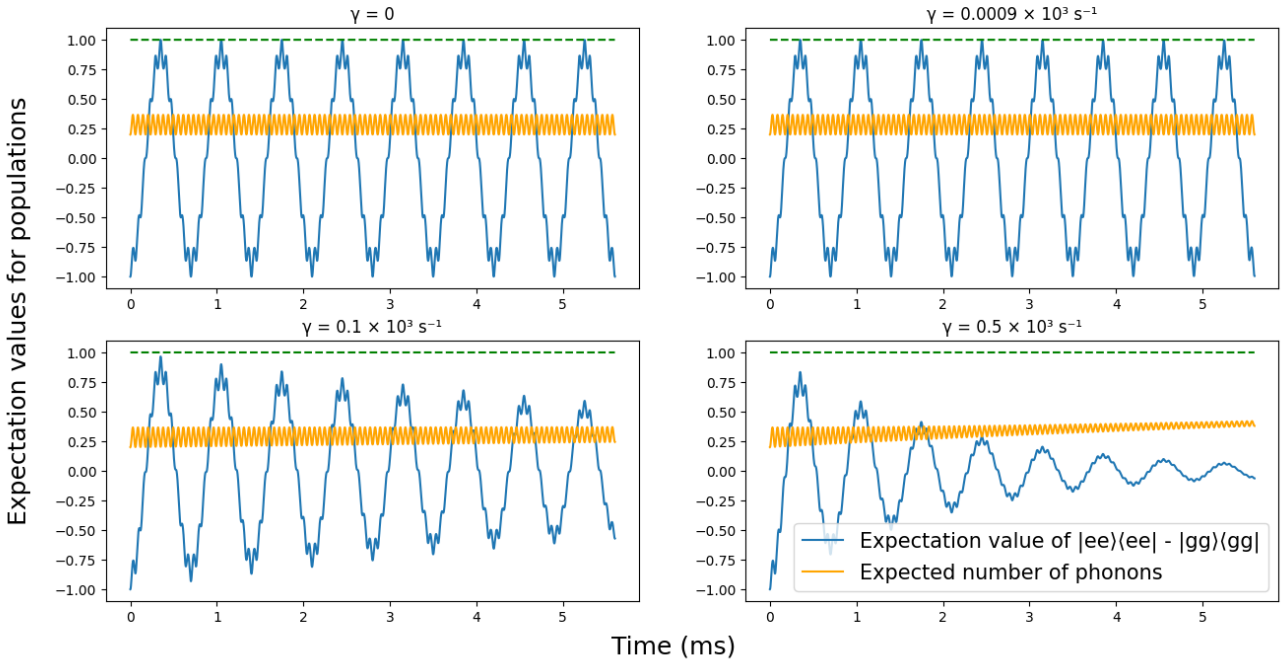


Figure 9: MS gate Rabi oscillations obtained for initial state $|gg\rangle$ in the presence of spontaneous emission for different decay rates γ . The top right graph shows the results obtained for the decay rate in the $^{40}\text{Ca}^+$ optical qubit. We observe that spontaneous emission has the effect of exponentially reducing the amplitude of oscillations over time. The plots are obtained using a Lindblad master equation solver in QuTip (the simulation used can be found on my [GitHub page](#)), where the Hamiltonian is taken to be the simplified form obtained in (19) after the second RWA is applied to kill the carrier and far off-resonant sidebands. The Lindblad collapse operator for spontaneous emission is given by $\hat{L}_{se} = \sqrt{\gamma}|g\rangle\langle e|$.

6.3 Dephasing

We consider here the effects of magnetic field and slow electric field noise on the system dynamics. We will consider each of these effects in turn, and will find that both will lead to *dephasing*, or *phase damping*, which we will derive in the following. First we consider the impacts of stray magnetic fields interacting with the ions. These will induce a magnetic dipole term in the Hamiltonian given by $-\vec{\mu} \cdot \vec{B}$, where $\vec{\mu}$ gives the magnetic moment of the ion for a given electronic state. Dephasing occurs when the strength of this \vec{B} field is not accounted for, and leads to the accumulation of relative phase between states with different $\vec{\mu}$ [3].

To illustrate the effects of phase damping, we take the qubit space spanned by $|g\rangle$ and $|e\rangle$, and assume for the moment that we have no external perturbation aside from the dephasing noise process we will consider, such that in the interaction picture both states will remain static with no phase accrual over time. Introducing now the magnetic dipole interaction, we assume the effect of this will be some non-zero additional energy splitting between these states such that in some time Δt , $|e\rangle$ will gain some additional phase $e^{i\theta_B}$ relative to $|g\rangle$. As a simplifying assumption, we take the \vec{B} field to vary in such a way that the parameter θ_B will become well-represented by a continuous random variable [1], and further, central limit theorem tells us that this will tend to a normal distribution for large times Δt . Thus, taking the mean to be 0 and the variance 2λ for this distribution, we can obtain the expectation for the resulting density matrix after time Δt :

$$\begin{aligned}
\rho(\Delta t) &= \frac{1}{\sqrt{4\pi\lambda}} \int_{-\infty}^{\infty} d\theta_B R_z(\theta_B) \rho(0) R_z^\dagger(\theta_B) \exp\left(-\frac{\theta_B^2}{4\lambda}\right) \\
&= \frac{1}{\sqrt{4\pi\lambda}} \int_{-\infty}^{\infty} d\theta_B \begin{pmatrix} 1 & 0 \\ 0 & e^{i\theta_B} \end{pmatrix} \begin{pmatrix} \rho_{00} & \rho_{01} \\ \rho_{10} & \rho_{11} \end{pmatrix} \begin{pmatrix} 1 & 0 \\ 0 & e^{-i\theta_B} \end{pmatrix} \exp\left(-\frac{\theta_B^2}{4\lambda}\right) \\
&= \frac{1}{\sqrt{4\pi\lambda}} \int_{-\infty}^{\infty} d\theta_B \begin{pmatrix} \rho_{00} & \rho_{01} e^{-i\theta_B} \\ \rho_{10} e^{i\theta_B} & \rho_{11} \end{pmatrix} \exp\left(-\frac{\theta_B^2}{4\lambda}\right) \\
&= \begin{pmatrix} \rho_{00} & \rho_{01} e^{-\lambda} \\ \rho_{10} e^{-\lambda} & \rho_{11} \end{pmatrix}
\end{aligned} \tag{72}$$

We infer from (72) that the result of dephasing will be exponential decay of off-diagonal elements of the density matrix, such that for large times Δt (and therefore large variance 2λ), any superposition state $\alpha|g\rangle + \beta|e\rangle$ will tend to the mixed state $|\alpha|^2|g\rangle\langle g| + |\beta|^2|e\rangle\langle e|$. This will result in the loss of any coherence properties of the superposition.

Applying this noise process to the MS gate dynamics, we obtain similar results to the plots obtained from spontaneous emission. The results can be seen in Figure 10. As with spontaneous emission, we see that phase damping has the effect of exponentially reducing the amplitude of oscillations over time, however, phase damping will differ from spontaneous emission in that rather than pulling each ion towards the ground state $|g\rangle$, the steady state solution for the density matrix of each ion will be the maximal entropy state $\frac{1}{2}(|g\rangle\langle g| + |e\rangle\langle e|)$. This solution arises physically due to the gradual loss of coherence between the $|g\rangle$ and $|e\rangle$ states, whilst Rabi oscillations of each ensure that we become equally probable to observe any state for either ion at large times. We also interestingly observe the gradual increase of the number of phonons over time. This arises by consequence of the decoherence between the $|g\rangle$ and $|e\rangle$ states causing the loop closure condition for the displacement operator to no longer be valid, such that the initial motional state is no longer cleanly recovered after every cycle.

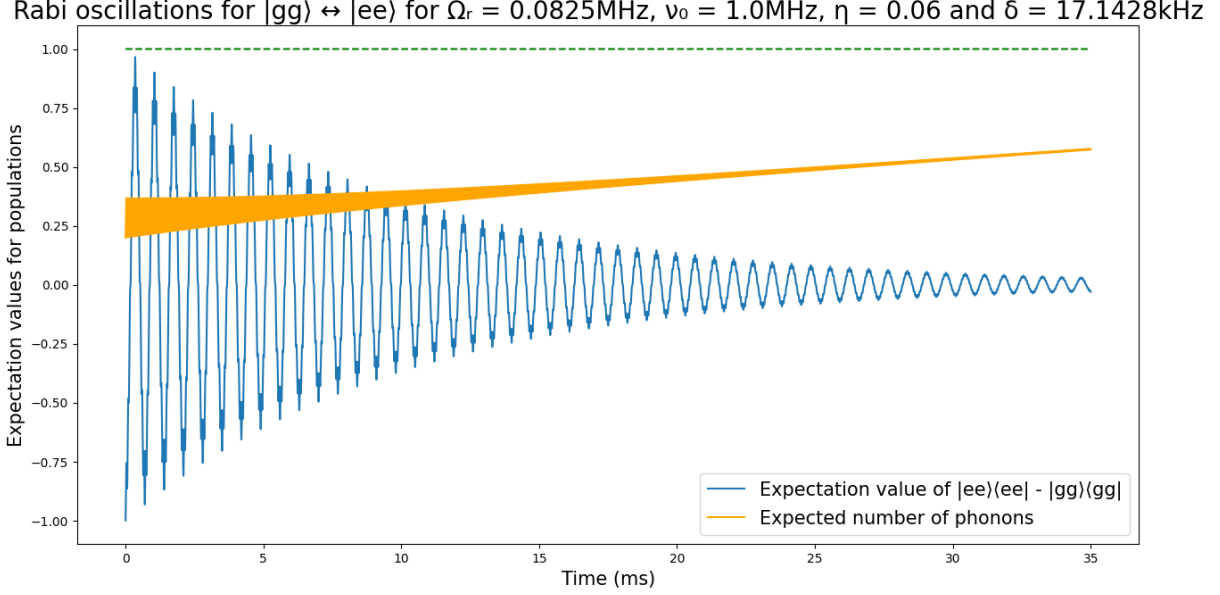


Figure 10: MS gate Rabi oscillations obtained for initial state $|gg\rangle$ in the presence of phase damping. The corresponding Lindblad operator is given by $\hat{L}_{pd} = \sqrt{\gamma}\hat{\sigma}_z$, where γ gives the rate of phase damping. This plot is obtained for a choice of $\gamma = 50\text{s}^{-1}$.

We have shown that stray fluctuating magnetic fields can lead to dephasing between the electronic qubit levels due to the magnetic dipole interaction. We now consider the effects of slow electric field noise, which will require reintroducing the previously neglected motional states of the ions to our model. The word slow in this context describes the frequency of the fluctuations relative to the trap frequencies $\sim \nu_0$. Fast electric field noise will be considered in the next subsection on motional heating, as we will find this has a physically different effect on the system.

Just as variations in the magnetic field resulted in small shifts of the energy splitting between the electronic qubit states $|g\rangle$ and $|e\rangle$, we find that small voltage fluctuations in the trap electrodes will lead to gradual changes in the allowed normal mode frequencies for the motion of ions within the trap [3][4]. Thus, the phonon energy spacing $\hbar\nu_0$ in the centre-of-mass mode used for the sideband transitions, as well as the energy spacings for other spectator modes will change. However, there is a critical distinction here from the magnetic dipole interaction case in that these variations will change not only the energies of the unperturbed Hamiltonian H_0 , but also the eigenbasis itself. Fortunately, in the limit of slow fluctuations, the adiabatic theorem tells us that states will track the instantaneous eigenbasis of H_0 as it changes, such that a given phonon state will remain in the corresponding phonon state of the changing motional Hamiltonian. The result will be a variation in the corresponding energies, which as seen before will lead to dephasing.

As an additional consequence of small variations in the trap frequency ν_0 , we also find that the detuning δ from the sidebands will also change [15]. For red and blue detuned laser frequencies $\omega_{L1} = \omega_0 - \nu_0 - \delta$ and $\omega_{L2} = \omega_0 + \nu_0 + \delta$ as defined in Section 3, we immediately obtain that a variation of $\nu_0 \rightarrow \nu_0 - \epsilon$ will yield equivalent dynamics to a symmetric detuning error of $\delta \rightarrow \delta + \epsilon$. The effect of this error source can therefore easily be understood by applying the analysis in Section 4; we will obtain a violation of the loop closure condition due to the additional phase accrual of ϵt_g . Consequently, we obtain a residual entanglement between the motional and electronic qubit subspaces at the gate time due to the state-dependent displacement $\hat{D}(\frac{\eta\Omega_R}{2(\delta+\epsilon)}(1 - e^{-i\epsilon t_g})\hat{S}_y^{(\phi)})$ [15].

As with spontaneous emission, it will become useful to obtain an operator-sum representation for this process. Note there is no unique set of operation elements to describe a given operation, and often different choices of operation elements can lend different insight into its structure. One choice [12] for representing the phase damping operation is the set given by:

$$E_0 = \begin{pmatrix} \sqrt{1-\gamma} & 0 \\ 0 & \sqrt{1-\gamma} \end{pmatrix}, \quad E_1 = \begin{pmatrix} \sqrt{\gamma} & 0 \\ 0 & 0 \end{pmatrix}, \quad E_2 = \begin{pmatrix} 0 & 0 \\ 0 & \sqrt{\gamma} \end{pmatrix}, \quad (73)$$

which by explicitly operating on ρ we see will recover the same results as (72):

$$\begin{aligned} \sum_j E_j \rho E_j^\dagger &= E_0 \rho E_0^\dagger + E_1 \rho E_1^\dagger + E_2 \rho E_2^\dagger \\ &= (1-\gamma) \begin{pmatrix} \rho_{00} & \rho_{01} \\ \rho_{10} & \rho_{11} \end{pmatrix} + \begin{pmatrix} \gamma \rho_{00} & 0 \\ 0 & 0 \end{pmatrix} + \begin{pmatrix} 0 & 0 \\ 0 & \gamma \rho_{11} \end{pmatrix} \\ &= \begin{pmatrix} \rho_{00} & \rho_{01}(1-\gamma) \\ \rho_{10}(1-\gamma) & \rho_{11} \end{pmatrix} \end{aligned} \quad (74)$$

Equating $(1-\gamma)$ from (74) and $e^{-\lambda}$ from (72) yields the correct mappings for the phase damping operation under this set of operation elements. This choice of representation can be interpreted physically as arising from elastic scattering of a photon, such that the ion has some probability γ in some arbitrary time interval of interacting elastically with its environment, which we will take to be some thermal bath of photons. Defining the initial state of the environment state to be given by $|0_E\rangle$, we consider the mappings $|g, 0_E\rangle \rightarrow \sqrt{1-\gamma}|g, 0_E\rangle + \sqrt{\gamma}|g, 1_E\rangle$ and $|e, 0_E\rangle \rightarrow \sqrt{1-\gamma}|e, 0_E\rangle + \sqrt{\gamma}|e, 2_E\rangle$, where $|1_E\rangle$ and $|2_E\rangle$ give the 2 possible states of the scattered photons in the environment after interacting with the ion in state $|g\rangle$ and $|e\rangle$ respectively. In this picture, when tracing over the environment space, E_0 will be the operation element obtained when the photon was unscattered whilst E_1 and E_2 will give the operation elements corresponding to the events where the photon was scattered. In the literature, often this alternative picture is used instead to represent the dephasing process, thus it is insightful to see explicitly how both pictures will lead to equivalent dynamics for the system.

6.4 Motional Heating

For faster electric field fluctuations, the adiabatic theorem can no longer be applied as above. When the frequency of these fluctuations becomes comparable to the trap frequencies $\sim \nu_0$, the result will instead be resonant driving of transitions between the different phonon states, such that the phonon population in different modes may be changed. This will cause heating of the motional state.

Sources of such heating include blackbody radiation (albeit to a very limited extent) and fundamental Johnson noise arising from the random motion of electrons in the electrodes at finite temperature [4][5]. However, the observed heating rates are typically much greater than the theoretical predictions arising from these two conventional sources, thus we conclude that there must exist other sources of heating unaccounted for. In the literature, this heating is referred to as *anomalous motional heating*, or AMH. Although the exact origin of AMH is still an active area of research, current models predict that AMH arises from surface effects [4] (rather than bulk properties) of the electrodes, and is largest for low frequencies, short surface-ion distances and high temperatures [5].

Figure 11 shows the gate dynamics in the presence of motional heating. We observe, as expected, that the phonon population will increase over time as a consequence of this heating. We find that

fidelity of the mapping is reduced from 0.9991 to 0.99614. In the following we will analyse the cause of this reduction in fidelity by considering the dynamics obtained from the corresponding Lindblad master equation.

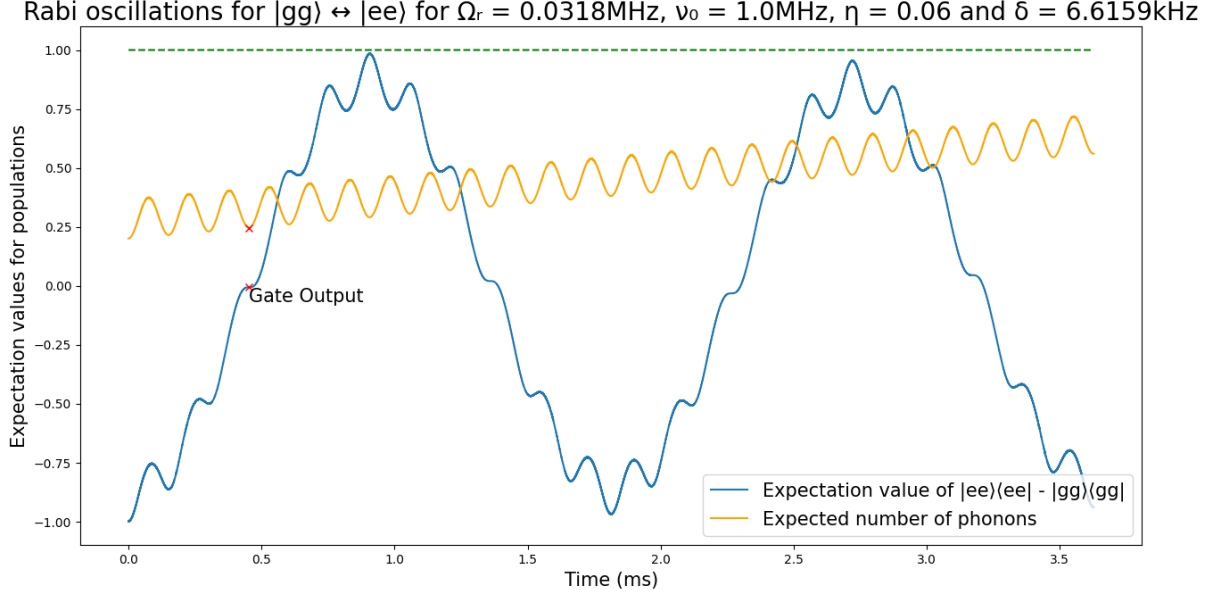


Figure 11: MS gate Rabi oscillations obtained for initial state $|gg\rangle$ in the presence of motional heating. The corresponding Lindblad operators are given by $\hat{L}_{heat} = \sqrt{100}\hat{a}^\dagger$ and $\hat{L}_{cool} = \sqrt{102}\hat{a}$.

We present in the following a derivation and analysis of the dynamics obtained under motional heating. We will follow loosely the method presented in [2] and [13]. The dynamics of the system will obey the Lindblad master equation with Hamiltonian given by the MS Hamiltonian for the bichromatic drive stated in (22), and with Lindblad operators for thermalisation with the environment given by $\hat{L}_{heat} = \sqrt{\gamma n_{th}}\hat{a}^\dagger$ and $\hat{L}_{cool} = \sqrt{\gamma(n_{th} + 1)}\hat{a}$. Here, γ gives the strength of the interaction with the thermal bath and n_{th} gives the number of phonons at equilibrium [2]. A more rigorous model of heating will also account for dephasing effects obtained for elastic photon scattering (analogously to the results of (73) and (74)) [13]. However, for pure thermalisation, the two Lindblad operators listed here will be sufficient to give a broad overview of the dominant effects of motional heating. Thus, for $\hat{L}_1 \equiv \hat{L}_{heat}$ and $\hat{L}_2 \equiv \hat{L}_{cool}$ as defined above, the resulting Lindblad equation will read:

$$\frac{d}{dt}\rho = -\frac{i}{\hbar}[H_{MS}, \rho] + \sum_{j=1}^2 (\hat{L}_j \rho \hat{L}_j^\dagger - \frac{1}{2}\{\hat{L}_j^\dagger \hat{L}_j, \rho\}) \quad (75)$$

We can simplify this problem by taking advantage of the fact that we already know the solution to $\rho(t)$ when evolving solely under Hamiltonian H_{MS} in the absence of the Lindblad terms, as this was solved for in Section 3. This motivates a frame transformation in order to remove the explicit H_{MS} dependence. As shown in Appendix A.1, if we apply the mappings:

$$\begin{aligned}
\rho &\rightarrow \tilde{\rho} \equiv U_{MS}^\dagger \rho U_{MS} \\
H_{MS} &\rightarrow \tilde{H}_{MS} \equiv U_{MS}^\dagger H_{MS} U_{MS} \\
\hat{L}_j &\rightarrow \hat{\tilde{L}}_j \equiv U_{MS}^\dagger \hat{L}_j U_{MS},
\end{aligned} \tag{76}$$

where U_{MS} is the MS evolution unitary obtained in (30), then (75) will instead read:

$$\frac{d}{dt} \tilde{\rho} = \sum_{j=1}^2 (\hat{\tilde{L}}_j \rho \hat{\tilde{L}}_j^\dagger - \frac{1}{2} \{ \hat{\tilde{L}}_j^\dagger \hat{\tilde{L}}_j, \rho \}) \tag{77}$$

Thus we only retain contributions from the Lindblad terms in this frame. To solve (77), we require the transformed Lindblad operators, proportional to the transformed creation and annihilation operators $\hat{\tilde{a}}^\dagger$ and $\hat{\tilde{a}}$. As a reminder, we restate U_{MS} given in (30):

$$U_{MS} = \exp\left(\frac{\eta\Omega_R}{2\delta} \hat{S}_y^{(\phi)}((e^{i\delta t} - 1)\hat{a} - (e^{-i\delta t} - 1)\hat{a}^\dagger)\right) \cdot \exp\left(-i\left(\frac{\eta\Omega_R}{2\delta}\right)^2 \hat{S}_y^{(\phi)2}(\delta t - \sin(\delta t))\right) \tag{78}$$

We note that only the first term (which we had previously referred to as the 'displacement operator') has non-commuting terms with \hat{a} and \hat{a}^\dagger . The second term, however, which previously we found was responsible for the entangling MS gate dynamics that we wanted, will not affect the motional state. Thus, only this first term will contribute to the frame transformations. For $\hat{\tilde{a}}^\dagger$:

$$\begin{aligned}
\hat{\tilde{a}}^\dagger &\equiv U_{MS}^\dagger \hat{a}^\dagger U_{MS} \\
&= \exp\left(\frac{\eta\Omega_R}{2\delta} \hat{S}_y^{(\phi)}((e^{-i\delta t} - 1)\hat{a}^\dagger - (e^{i\delta t} - 1)\hat{a})\right) \hat{a}^\dagger \exp\left(\frac{\eta\Omega_R}{2\delta} \hat{S}_y^{(\phi)}((e^{i\delta t} - 1)\hat{a} - (e^{-i\delta t} - 1)\hat{a}^\dagger)\right)
\end{aligned} \tag{79}$$

To solve this, we apply the Campbell identity:

$$e^X Y e^{-X} = Y + [X, Y] + \frac{1}{2!} [X, [X, Y]] + \frac{1}{3!} [X, [X, [X, Y]]] + \dots \tag{80}$$

This yields:

$$\begin{aligned}
\hat{\tilde{a}}^\dagger &= \exp\left(\frac{\eta\Omega_R}{2\delta} \hat{S}_y^{(\phi)}((e^{-i\delta t} - 1)\hat{a}^\dagger - (e^{i\delta t} - 1)\hat{a})\right) \hat{a}^\dagger \exp\left(\frac{\eta\Omega_R}{2\delta} \hat{S}_y^{(\phi)}((e^{i\delta t} - 1)\hat{a} - (e^{-i\delta t} - 1)\hat{a}^\dagger)\right) \\
&= \hat{a}^\dagger + \left[\frac{\eta\Omega_R}{2\delta} \hat{S}_y^{(\phi)}((e^{-i\delta t} - 1)\hat{a}^\dagger - (e^{i\delta t} - 1)\hat{a}), \hat{a}^\dagger\right] + \dots \\
&= \hat{a}^\dagger - \frac{\eta\Omega_R}{2\delta} \hat{S}_y^{(\phi)}(e^{i\delta t} - 1)[\hat{a}, \hat{a}^\dagger] + \dots \\
&= \hat{a}^\dagger - \frac{\eta\Omega_R}{2\delta} \hat{S}_y^{(\phi)}(e^{i\delta t} - 1)
\end{aligned} \tag{81}$$

The final line is obtained after recognising that all higher order commutators in (80) will vanish as the first order term is found to be proportional to the identity \mathbb{I} , and all higher order terms are obtained from commutators with this term. Applying the same procedure to $\hat{\tilde{a}}$:

$$\hat{\tilde{a}} = \hat{a} - \frac{\eta\Omega_R}{2\delta}\hat{S}_y^{(\phi)}(e^{-i\delta t} - 1) \quad (82)$$

From (81) and (82), we are now able to solve explicitly for solutions of (77):

$$\begin{aligned} \frac{d}{dt}\tilde{\rho} &= \gamma n_{th}(\hat{a}^\dagger \tilde{\rho} \hat{a} - \frac{1}{2}\{\hat{a}\hat{a}^\dagger, \tilde{\rho}\}) + \gamma(n_{th} + 1)(\hat{a} \tilde{\rho} \hat{a}^\dagger - \frac{1}{2}\{\hat{a}^\dagger \hat{a}, \tilde{\rho}\}) \\ &= \gamma n_{th}((\hat{a}^\dagger - \frac{\eta\Omega_R}{2\delta}\hat{S}_y^{(\phi)}(e^{i\delta t} - 1))\tilde{\rho}(\hat{a} - \frac{\eta\Omega_R}{2\delta}\hat{S}_y^{(\phi)}(e^{-i\delta t} - 1)) \\ &\quad - \frac{1}{2}\{(\hat{a} - \frac{\eta\Omega_R}{2\delta}\hat{S}_y^{(\phi)}(e^{-i\delta t} - 1))(\hat{a}^\dagger - \frac{\eta\Omega_R}{2\delta}\hat{S}_y^{(\phi)}(e^{i\delta t} - 1)), \tilde{\rho}\}) \\ &\quad + \gamma(n_{th} + 1)((\hat{a} - \frac{\eta\Omega_R}{2\delta}\hat{S}_y^{(\phi)}(e^{-i\delta t} - 1))\tilde{\rho}(\hat{a}^\dagger - \frac{\eta\Omega_R}{2\delta}\hat{S}_y^{(\phi)}(e^{i\delta t} - 1)) \\ &\quad - \frac{1}{2}\{(\hat{a}^\dagger - \frac{\eta\Omega_R}{2\delta}\hat{S}_y^{(\phi)}(e^{i\delta t} - 1))(\hat{a} - \frac{\eta\Omega_R}{2\delta}\hat{S}_y^{(\phi)}(e^{-i\delta t} - 1)), \tilde{\rho}\}) \end{aligned} \quad (83)$$

As a simplifying assumption, we will take the initial state of ρ (equivalently also for $\tilde{\rho}$ as these will be the same at $t = 0$) to be given by $\rho(0) = \rho_{el}(0) \otimes \sum_n P_n(0)|n\rangle\langle n|$, where ρ_{el} gives the reduced density matrix of the electronic subspace obtained when tracing over the phonon states. To obtain this result, we have firstly taken the electronic and motional states to be initially separable and therefore uncorrelated, then secondly we have further assumed that the motional state ρ_{mot} is given by a diagonal density matrix in the Fock basis. This assumption can be justified after considering the effects of previously considered noise effects, where decoherence will eliminate off-diagonal elements of ρ_{mot} . We will find that this will allow us to disregard certain terms in (83), as when we later trace over the motional space to just obtain the dynamics of the qubit states ρ_{el} , these terms will disappear due to the absence of any off-diagonal elements of ρ_{mot} :

$$\begin{aligned} \frac{d}{dt}\tilde{\rho} &= \gamma n_{th}((\hat{a}^\dagger \tilde{\rho} \hat{a} + (\frac{\eta\Omega_R}{2\delta})^2(e^{i\delta t} - 1)(e^{-i\delta t} - 1)\hat{S}_y^{(\phi)}\tilde{\rho}\hat{S}_y^{(\phi)}) \\ &\quad - \frac{1}{2}(\hat{a}\hat{a}^\dagger \tilde{\rho} + (\frac{\eta\Omega_R}{2\delta})^2(e^{i\delta t} - 1)(e^{-i\delta t} - 1)\hat{S}_y^{(\phi)2}\tilde{\rho}) \\ &\quad - \frac{1}{2}(\tilde{\rho}\hat{a}\hat{a}^\dagger + (\frac{\eta\Omega_R}{2\delta})^2(e^{i\delta t} - 1)(e^{-i\delta t} - 1)\tilde{\rho}\hat{S}_y^{(\phi)2})) \\ &\quad + \gamma(n_{th} + 1)((\hat{a}\tilde{\rho}\hat{a}^\dagger + (\frac{\eta\Omega_R}{2\delta})^2(e^{i\delta t} - 1)(e^{-i\delta t} - 1)\hat{S}_y^{(\phi)}\tilde{\rho}\hat{S}_y^{(\phi)}) \\ &\quad - \frac{1}{2}(\hat{a}^\dagger \hat{a}\tilde{\rho} + (\frac{\eta\Omega_R}{2\delta})^2(e^{i\delta t} - 1)(e^{-i\delta t} - 1)\hat{S}_y^{(\phi)2}\tilde{\rho}) \\ &\quad - \frac{1}{2}(\tilde{\rho}\hat{a}^\dagger \hat{a} + (\frac{\eta\Omega_R}{2\delta})^2(e^{i\delta t} - 1)(e^{-i\delta t} - 1)\tilde{\rho}\hat{S}_y^{(\phi)2})) \\ &\quad + \dots, \end{aligned} \quad (84)$$

where \dots contains terms containing $\hat{a}\tilde{\rho}$ or $\hat{a}^\dagger\tilde{\rho}$ that will lead to off-diagonal elements of $\tilde{\rho}_{mot}$. Clearly, when tracing over the motional space, these terms will not contribute to the dynamics of $\tilde{\rho}_{el}$, as can be seen in the following:

$$\begin{aligned}
\sum_n \langle n | \hat{a} \tilde{\rho} | n \rangle &= \sum_n \sqrt{n} \rho_{el} \langle n-1 | (\sum_m P_m | m \rangle \langle m |) | n \rangle \\
&= \sum_{n,m} \sqrt{n} P_m \rho_{el} \langle n-1 | m \rangle \langle m | n \rangle \\
&= 0,
\end{aligned} \tag{85}$$

and similarly for $tr_{mot}(\hat{a}^\dagger \tilde{\rho})$. Tracing over the remaining terms in (84), we obtain:

$$\begin{aligned}
\frac{d}{dt} \tilde{\rho}_{el} &= tr_{mot}(\gamma n_{th} ((\hat{a}^\dagger \tilde{\rho} \hat{a} - \frac{1}{2}(\hat{a} \hat{a}^\dagger \tilde{\rho}) - \frac{1}{2}(\tilde{\rho} \hat{a} \hat{a}^\dagger)) \\
&\quad + (\frac{\eta \Omega_R}{2\delta})^2 (e^{i\delta t} - 1)(e^{-i\delta t} - 1)(\hat{S}_y^{(\phi)} \tilde{\rho} \hat{S}_y^{(\phi)} - \frac{1}{2} \hat{S}_y^{(\phi)2} \tilde{\rho} - \frac{1}{2} \tilde{\rho} \hat{S}_y^{(\phi)2})) \\
&\quad + \gamma(n_{th} + 1)((\hat{a} \tilde{\rho} \hat{a}^\dagger - \frac{1}{2}(\hat{a}^\dagger \hat{a} \tilde{\rho}) - \frac{1}{2}(\tilde{\rho} \hat{a}^\dagger \hat{a})) \\
&\quad + (\frac{\eta \Omega_R}{2\delta})^2 (e^{i\delta t} - 1)(e^{-i\delta t} - 1)(\hat{S}_y^{(\phi)} \tilde{\rho} \hat{S}_y^{(\phi)} - \frac{1}{2} \hat{S}_y^{(\phi)2} \tilde{\rho} - \frac{1}{2} \tilde{\rho} \hat{S}_y^{(\phi)2}))) \\
&= 2\gamma(2n_{th} + 1)(\frac{\eta \Omega_R}{2\delta})^2 (1 - \cos(\delta t)) (\hat{S}_y^{(\phi)} \tilde{\rho}_{el} \hat{S}_y^{(\phi)} - \frac{1}{2} \hat{S}_y^{(\phi)2} \tilde{\rho}_{el} - \frac{1}{2} \tilde{\rho}_{el} \hat{S}_y^{(\phi)2}),
\end{aligned} \tag{86}$$

where terms acting on the motional space have cancelled completely by consequence of the cyclic property $tr(AB) = tr(BA)$. The resulting differential equation obtained in (86) is most easily solved by working in the eigenbasis of $\hat{S}_y^{(\phi)}$, which we denote by the set $\{|M\rangle\}$, such that the resulting equations are fully decoupled [2]. Thus, taking $\tilde{\rho}_{el} = \sum_{M,M'} |M\rangle \tilde{\rho}_{M,M'} \langle M'|$ (where we have now dropped the el subscript from $\tilde{\rho}_{M,M'}$ for notational convenience), we obtain the following decoupled system of equations:

$$\begin{aligned}
\frac{d}{dt} \tilde{\rho}_{M,M'} &= 2\gamma(2n_{th} + 1)(\frac{\eta \Omega_R}{2\delta})^2 (1 - \cos(\delta t)) (MM' - \frac{1}{2}M^2 - \frac{1}{2}M'^2) \tilde{\rho}_{M,M'} \\
&= -\gamma(2n_{th} + 1)(\frac{\eta \Omega_R}{2\delta})^2 (1 - \cos(\delta t)) (M - M')^2 \tilde{\rho}_{M,M'}
\end{aligned} \tag{87}$$

$$\implies \tilde{\rho}_{M,M'}(t) = \tilde{\rho}_{M,M'}(0) \exp(-\gamma(2n_{th} + 1)(\frac{\eta \Omega_R}{2\delta})^2 (t - \frac{1}{\delta} \sin(\delta t)) (M - M')^2) \tag{88}$$

Lastly, after enforcing loop closure $\delta t = 2\pi m$ for integer m , this reduces to the simpler form:

$$\tilde{\rho}_{M,M'}(t) = \tilde{\rho}_{M,M'}(0) \exp(-\gamma(2n_{th} + 1)(\frac{\eta \Omega_R}{2\delta})^2 (M - M')^2 t) \tag{89}$$

We therefore obtain that the primary result of motional heating on the qubit subspace will be decoherence between the eigenstates of $\hat{S}_y^{(\phi)}$. To leading order, we observe that the rate of this decoherence will scale quadratically with the quantity $\frac{\eta \Omega_R}{2\delta}$, which from Section 4 we identify as the magnitude of displacements of the phonon states in phase-space [15]. This motivates one possible solution for reducing the effect of heating of reducing this factor of $\frac{\eta \Omega_R}{2\delta}$ in order to cause the phonon states to traverse many smaller circular trajectories [15], as opposed to fewer larger circular trajectories. For the simple bichromatic drive discussed in this paper, this is most practically achieved by increasing the loop closure parameter m . To see how this results in a reduction in the impacts of heating to fidelity, we recall from Section 4 the relation $\delta = 2\Omega_R \eta \sqrt{m}$, which we obtained from the loop closure requirement $\delta t_g = 2\pi m$. Inserting this into (89), we obtain at the gate time:

$$\tilde{\rho}_{M,M'}(t_g) = \tilde{\rho}_{M,M'}(0) \exp\left(-\frac{\alpha(M - M')^2}{\sqrt{m}}\right), \quad (90)$$

where all other parameters have been absorbed into the constant of proportionality α . Figure 12 demonstrates how increasing this parameter m to allow for more loops in phase space leads to a reduction in the infidelity resulting from heating. However, this solution has the fairly significant disadvantage of increasing the time taken to perform the gate, which will scale with \sqrt{m} . More sophisticated techniques to reduce the effects of heating without sacrificing gate time can be found in [13] and [15], where the strategy employed here is to use multitone driving (as opposed to the simple bichromatic case considered here) in order to engineer different phase-space trajectories that involve smaller excursions from the origin. These techniques are however beyond the scope of this review, so we will terminate our discussion of heating here.

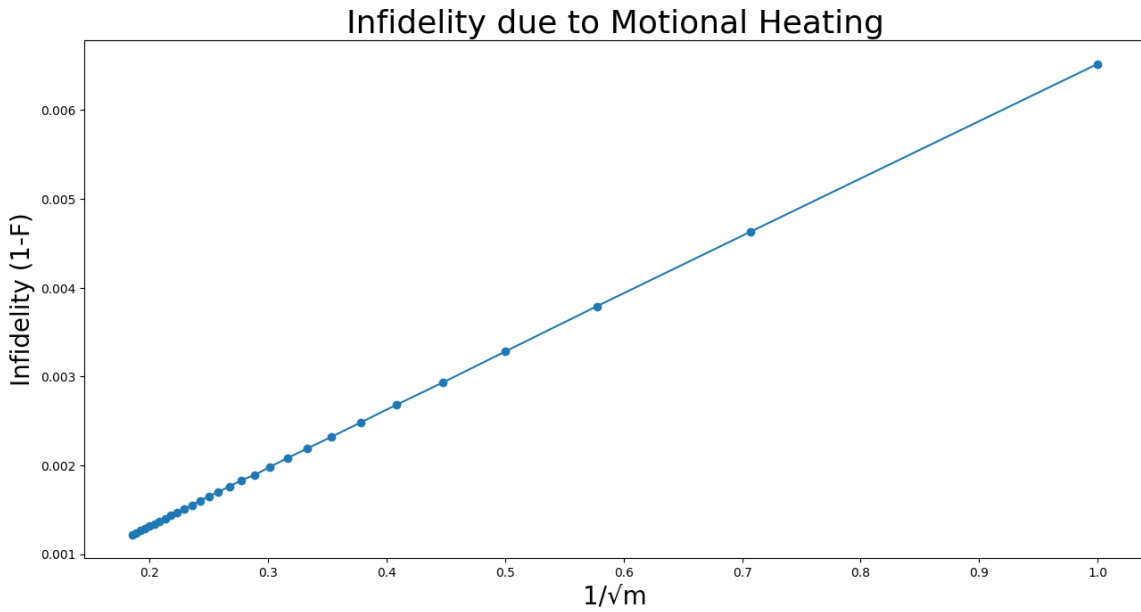


Figure 12: We observe that larger values of m (or equivalently, smaller values of $\frac{1}{\sqrt{m}}$) will result in higher fidelity (lower infidelity) mappings in the presence of heating. As with all previous cases in this review, the values for infidelity are obtained for the specific case of input $|gg\rangle$ by comparing the state at the gate time to the required output of $\frac{|gg\rangle - i|ee\rangle}{\sqrt{2}}$. The gate is simulated using a numerical Lindblad master equation solver using the simplified MS Hamiltonian given in (22), as well as with the previously stated Lindblad operators for heating and cooling. To leading order, we obtain a linear relation, which is consistent with the predictions of (90), as well as with the claims of [2].

7 Construction of CNOT

In this final section, we construct the CNOT gate using a combination of the MS gate obtained in Section 3 and single-qubit unitaries. Although the universality criteria for quantum computing requires only single qubit unitaries and *any* two-qubit entangling unitary (including of course the MS gate), it is still insightful to see explicitly how we can construct CNOT from this gate, as CNOT is more often used in proofs demonstrating universality, and explicitly features in many schematics of various quantum algorithms. Thus, whilst the ability to construct CNOT follows immediately from

the property of universality, it is still useful to see *how* this can be constructed, as this provides further insight into the behaviour of the MS gate.

We begin by restating the form of the MS unitary presented at the start of Section 3:

$$U_{MS} = \frac{1}{\sqrt{2}} \begin{pmatrix} 1 & 0 & 0 & -i \\ 0 & 1 & -i & 0 \\ 0 & -i & 1 & 0 \\ -i & 0 & 0 & 1 \end{pmatrix} \quad (91)$$

By inspection, we see that the diagonal basis $\{|\pm\pm\rangle\}$ defined by $|\pm_1\pm_2\rangle \equiv \frac{1}{\sqrt{2}}(|g\rangle\pm_1|e\rangle) \otimes \frac{1}{\sqrt{2}}(|g\rangle\pm_2|e\rangle)$ will diagonalise this unitary. Expressing in this basis, we obtain:

$$U_{MS} = e^{-\frac{i\pi}{4}} \begin{pmatrix} 1 & 0 & 0 & 0 \\ 0 & i & 0 & 0 \\ 0 & 0 & i & 0 \\ 0 & 0 & 0 & 1 \end{pmatrix} \quad (92)$$

Disregarding the global phase, this unitary can be shown to be equivalent to a controlled phase (C-Z) gate up to a global rotation about the z-axis [3].

$$\begin{aligned} \hat{R}_z(-\frac{\pi}{2})U_{MS} &= \begin{pmatrix} 1 & 0 \\ 0 & e^{-\frac{i\pi}{2}} \end{pmatrix} \otimes \begin{pmatrix} 1 & 0 \\ 0 & e^{-\frac{i\pi}{2}} \end{pmatrix} \begin{pmatrix} 1 & 0 & 0 & 0 \\ 0 & i & 0 & 0 \\ 0 & 0 & i & 0 \\ 0 & 0 & 0 & 1 \end{pmatrix} \\ &= \begin{pmatrix} 1 & 0 & 0 & 0 \\ 0 & -i & 0 & 0 \\ 0 & 0 & -i & 0 \\ 0 & 0 & 0 & -1 \end{pmatrix} \begin{pmatrix} 1 & 0 & 0 & 0 \\ 0 & i & 0 & 0 \\ 0 & 0 & i & 0 \\ 0 & 0 & 0 & 1 \end{pmatrix} \\ &= \begin{pmatrix} 1 & 0 & 0 & 0 \\ 0 & 1 & 0 & 0 \\ 0 & 0 & 1 & 0 \\ 0 & 0 & 0 & -1 \end{pmatrix} \\ &= \text{C-Z} \end{aligned} \quad (93)$$

Thus, we obtain a controlled phase gate, defined by the controlled operation of applying $\hat{\sigma}_z$ on the second qubit controlled on the value of the first qubit. To convert this into CNOT, we use the identity $\hat{X} = \hat{H}\hat{Z}\hat{H}$, where \hat{H} is the Hadamard operator [1], to show that $\text{CNOT} = (\mathbb{I} \otimes \hat{H})\text{C-Z}(\mathbb{I} \otimes \hat{H})$:

$$\begin{aligned} (\mathbb{I} \otimes \hat{H})\hat{R}_z(-\frac{\pi}{2})U_{MS}(\mathbb{I} \otimes \hat{H}) &= \frac{1}{2} \begin{pmatrix} 1 & 1 & 0 & 0 \\ 1 & -1 & 0 & 0 \\ 0 & 0 & 1 & 1 \\ 0 & 0 & 1 & -1 \end{pmatrix} \begin{pmatrix} 1 & 0 & 0 & 0 \\ 0 & 1 & 0 & 0 \\ 0 & 0 & 1 & 0 \\ 0 & 0 & 0 & -1 \end{pmatrix} \begin{pmatrix} 1 & 1 & 0 & 0 \\ 1 & -1 & 0 & 0 \\ 0 & 0 & 1 & 1 \\ 0 & 0 & 1 & -1 \end{pmatrix} \\ &= \begin{pmatrix} 1 & 0 & 0 & 0 \\ 0 & 1 & 0 & 0 \\ 0 & 0 & 0 & 1 \\ 0 & 0 & 1 & 0 \end{pmatrix} \\ &= \text{CNOT} \end{aligned} \quad (94)$$

We note that it is only at this final step when converting from a controlled-phase gate into CNOT that we first require the ability to address a particular qubit in isolation without globally illuminating both ions with the laser. The MS gate itself (as well as its conversion into the controlled-phase gate) involves only global beams, thus eliminating the need to independently focus lasers on individual ions for its execution [3][4], which is a hugely experimentally favourable property of the gate.

8 Bibliography

- [1] Nielsen M. and Chuang I. (2010) *Quantum Computation and Quantum Information* Cambridge United Kingdom, Cambridge University Press
- [2] Sørensen A. and Mølmer K. (2000) *Entanglement and quantum computation with ions in thermal motion* arXiv:quant-ph/0002024v2 [quant-ph]
- [3] Häffner H., Roos C.F. and Blatt R. (2008) *Quantum computing with trapped ions* arXiv:0809.4368 [quant-ph]
- [4] Bruzewicz C.D., Chiaverini J., McConnell R. and Sage J. M. (2019) *Trapped-Ion Quantum Computing: Progress and Challenges* arXiv:1904.04178v1 [quant-ph]
- [5] Brownnutt M., Kumph M., Rabl P. and Blatt R. (2014) *Ion-trap measurements of electric-field noise near surfaces* arXiv:1409.6572v1 [quant-ph]
- [6] Roos C.F. (2008) *Ion trap quantum gates with amplitude-modulated laser beams* New J. Phys. 10 013002
- [7] Kirchmair G., Benhelm J., Zähringer F., Gerritsma R., Roos C.F. and Blatt R. (2009) *Deterministic entanglement of ions in thermal states of motion* arXiv:0810.0670 [quant-ph]
- [8] Blanes S., Casas F., Oteo J.A. and Ros J. (2008) *The Magnus expansion and some of its applications* arXiv:0810.5488v1 [math-ph]
- [9] Grynberg G., Aspect A. and Fabre C. (2010) *Introduction to Quantum Optics* Cambridge United Kingdom, Cambridge University Press
- [10] Schäfer V.M., Ballance C.J., Thirumalai K., Stephenson L.J., Ballance T.G., Steane A.M. and Lucas D.M. (2018) *Fast quantum logic gates with trapped-ion qubits* arXiv:1709.06952v2 [quant-ph]
- [11] Schindler P. *et al* (2013) *A quantum information processor with trapped ions* New J. Phys. 15 123012
- [12] Preskill J. (1998) *Lecture Notes for Physics 229: Quantum Information and Computation* California Institute of Technology
- [13] Haddadfarshi F. and Mintert F. (2016) *High fidelity quantum gates in the presence of motional heating* New J. Phys. 18 123007
- [14] Gerry C. and Knight P. (2005) *Introductory Quantum Optics* Cambridge, New York, Cambridge University Press
- [15] Webb A.E. *et al* (2018) *Resilient entangling gates for trapped ions* arXiv:1805.07351v1 [quant-ph]

A Appendix

A.1 Von Neumann equation in the Interaction Picture

The von Neumann equation for the time-evolution of some density operator ρ under some Hamiltonian H is given by:

$$\frac{d}{dt}\rho = -\frac{i}{\hbar}[H, \rho] \quad (95)$$

For $H = H_0 + H_{int}$, where H_0 gives the unperturbed core Hamiltonian of the system and H_{int} describes interactions with the environment, it is common to transform into a frame rotating with H_0 to simplify the problem. This frame is sometimes called the *interaction picture*, and taking H_0 to be time-independent, transformations into it can be achieved through the mappings:

$$\begin{aligned} \rho &\rightarrow \tilde{\rho} \equiv \exp\left(\frac{iH_0t}{\hbar}\right) \rho \exp\left(\frac{-iH_0t}{\hbar}\right) \\ H_{int} &\rightarrow \tilde{H}_{int} \equiv \exp\left(\frac{iH_0t}{\hbar}\right) H_{int} \exp\left(\frac{-iH_0t}{\hbar}\right) \end{aligned} \quad (96)$$

In the following we will derive the resulting dynamical equation for time-evolution of $\tilde{\rho}$. After solving this equation, we can then obtain time-evolution of the original density matrix ρ by simple reversal of the unitary transformation given in (96). The motivation for this whole procedure is that it is typically much easier to work in the interaction picture than to directly solve (95) with the full Hamiltonian H . This is because we will find that in the interaction picture, the phase evolution of eigenstates of H_0 will become absorbed into the definitions of \tilde{H}_{int} and $\tilde{\rho}$ such that explicit dependence on H_0 disappears.

$$\begin{aligned} \frac{d}{dt}\tilde{\rho} &= \frac{d}{dt}\left(\exp\left(\frac{iH_0t}{\hbar}\right) \rho \exp\left(\frac{-iH_0t}{\hbar}\right)\right) \\ &= \frac{iH_0}{\hbar}\tilde{\rho} + e^{\frac{iH_0t}{\hbar}}\left(\frac{d}{dt}\rho\right)e^{-\frac{iH_0t}{\hbar}} - \tilde{\rho}\frac{iH_0}{\hbar} \\ &= \frac{i}{\hbar}[H_0, \tilde{\rho}] + e^{\frac{iH_0t}{\hbar}}\left(-\frac{i}{\hbar}[H, \rho]\right)e^{-\frac{iH_0t}{\hbar}} \quad (\text{from (95)}) \\ &= \frac{i}{\hbar}[H_0, \tilde{\rho}] + e^{\frac{iH_0t}{\hbar}}\left(-\frac{i}{\hbar}[H_0 + H_{int}, \rho]\right)e^{-\frac{iH_0t}{\hbar}} \\ &= \frac{i}{\hbar}[H_0, \tilde{\rho}] - \frac{i}{\hbar}[H_0, \tilde{\rho}] - \frac{i}{\hbar}e^{\frac{iH_0t}{\hbar}}[H_{int}, \rho]e^{-\frac{iH_0t}{\hbar}} \quad (\text{as } [H_0, H_0] = 0) \\ &= -\frac{i}{\hbar}[\tilde{H}_{int}, \tilde{\rho}] \end{aligned} \quad (97)$$

A.2 Displacement Operator in Phase-Space

In Section 3.1, the MS gate unitary $U_{MS}(t)$ was derived and the result was stated in (30). We observed that the first term yielded dynamics that coupled the motional phonon subspace to the internal qubit states of each ion, given by:

$$\exp\left(\frac{\eta\Omega_R}{2\delta}\hat{S}_y^{(\phi)}((e^{i\delta t} - 1)\hat{a} - (e^{-i\delta t} - 1)\hat{a}^\dagger)\right) \quad (98)$$

In this section, we will analyse in more detail this term, which we will call the 'displacement operator', a name that is derived from quantum optics. In particular, we will obtain an interpretation of this operator as having the effect of displacing the motional state of the phonons in phase-space.

In quantum optics [14], the displacement operator $\hat{D}(\alpha)$ is defined by:

$$\hat{D}(\alpha) \equiv \exp(\alpha \hat{a}^\dagger - \alpha^* \hat{a}) \quad (99)$$

Comparing with (98) and for the moment looking only at the motional space (the effect of the $\hat{S}_y^{(\phi)}$ term in coupling the motional and electronic qubit subspaces is discussed in Section 4), we therefore justify calling this term a displacement operator by taking $\alpha = \frac{\eta \Omega_R}{2\delta} (1 - e^{-i\delta t})$. To understand the effect of this operator, we first define the coherent state $|\alpha\rangle$, defined by eigenstates of the annihilation operator [14]:

$$\hat{a}|\alpha\rangle = \alpha|\alpha\rangle \quad (100)$$

These states provide a natural way to motivate the phase-space interpretation of $\hat{D}(\alpha)$, as we will see in the following. We define rescaled position and momentum operators \hat{X}_1 and \hat{X}_2 [14] given by:

$$\begin{aligned} \hat{X}_1 &\equiv \frac{1}{2}(\hat{a} + \hat{a}^\dagger) \\ \hat{X}_2 &\equiv \frac{1}{2i}(\hat{a} - \hat{a}^\dagger) \end{aligned} \quad (101)$$

Taking expectation values of these operators for coherent states:

$$\begin{aligned} \langle \hat{X}_1 \rangle_\alpha &= \frac{1}{2}(\langle \alpha | \hat{a} | \alpha \rangle + \langle \alpha | \hat{a}^\dagger | \alpha \rangle) = \frac{1}{2}(\alpha + \alpha^*) = \text{Re}(\alpha) \\ \langle \hat{X}_2 \rangle_\alpha &= \frac{1}{2i}(\langle \alpha | \hat{a} | \alpha \rangle - \langle \alpha | \hat{a}^\dagger | \alpha \rangle) = \frac{1}{2i}(\alpha - \alpha^*) = \text{Im}(\alpha) \end{aligned} \quad (102)$$

Thus, the parameter α gives the rescaled phase-space coordinates of the state $|\alpha\rangle$ in the complex plane [14]. Note due to the uncertainty principle, states cannot occupy points in phase-space as with the classical-case, but instead will cover some region defined by a probability distribution. For coherent states, the shape of the resulting distribution will always be the same (a Gaussian) [14], and will differ only in position, where the coordinates $\langle \hat{X}_1 \rangle$ and $\langle \hat{X}_2 \rangle$ will give the centre of this distribution.

To analyse the coherent states $|\alpha\rangle$ further, it will be useful to express them as a linear combination of Fock states. We see that the following definition satisfies (100):

$$|\alpha\rangle \equiv e^{-\frac{1}{2}|\alpha|^2} \sum_{n=0}^{\infty} \frac{\alpha^n}{\sqrt{n!}} |n\rangle \quad (103)$$

$$\begin{aligned}
\Rightarrow \hat{a}|\alpha\rangle &\equiv e^{-\frac{1}{2}|\alpha|^2} \sum_{n=0}^{\infty} \frac{\alpha^n}{\sqrt{n!}} \hat{a}|n\rangle \\
&= e^{-\frac{1}{2}|\alpha|^2} \sum_{n=1}^{\infty} \frac{\alpha^n}{\sqrt{n!}} \sqrt{n}|n-1\rangle \\
&= e^{-\frac{1}{2}|\alpha|^2} \alpha \sum_{n=1}^{\infty} \frac{\alpha^{(n-1)}}{\sqrt{(n-1)!}} |n-1\rangle \\
&= \alpha|\alpha\rangle, \text{ as required.}
\end{aligned} \tag{104}$$

We will now show that the displacement operator $\hat{D}(\alpha)$ will have the effect of mapping the ground state $|0\rangle$ to the coherent state $|\alpha\rangle$ [14]. First, it will be useful to re-express $\hat{D}(\alpha)$ into a more convenient form. To do this, we apply the Baker-Campbell-Hausdorff (BCH) formula:

$$\exp(A)\exp(B) = \exp\left(A + B + \frac{1}{2}[A, B] + \dots\right), \tag{105}$$

where higher order terms contain nested commutators containing $[A, B]$. Taking $A \equiv \alpha\hat{a}^\dagger$ and $B \equiv -\alpha^*\hat{a}$, we obtain:

$$[A, B] = [\alpha\hat{a}^\dagger, -\alpha^*\hat{a}] = |\alpha|^2\mathbb{I}, \tag{106}$$

and thus all higher order commutators must vanish. By extension, as $[A, [A, B]] = [B, [A, B]] = 0$, we can also separate out the exponential in (105) as follows:

$$\exp\left(A + B + \frac{1}{2}[A, B] + \dots\right) = \exp(A + B)\exp\left(\frac{1}{2}[A, B]\right) \tag{107}$$

Applying this result to (99):

$$\begin{aligned}
\hat{D}(\alpha) &= \exp(\alpha\hat{a}^\dagger - \alpha^*\hat{a}) \\
&= \exp(\alpha\hat{a}^\dagger)\exp(-\alpha^*\hat{a})e^{-\frac{1}{2}|\alpha|^2}
\end{aligned} \tag{108}$$

Expressed in this form, we can now operate on $|0\rangle$:

$$\begin{aligned}
\hat{D}(\alpha)|0\rangle &= \exp(\alpha\hat{a}^\dagger)\exp(-\alpha^*\hat{a})e^{-\frac{1}{2}|\alpha|^2}|0\rangle \\
&= e^{-\frac{1}{2}|\alpha|^2}\exp(\alpha\hat{a}^\dagger)(\mathbb{I} - \alpha^*\hat{a} + \dots)|0\rangle \\
&= e^{-\frac{1}{2}|\alpha|^2}\exp(\alpha\hat{a}^\dagger)|0\rangle \\
&= e^{-\frac{1}{2}|\alpha|^2} \sum_{n=0}^{\infty} \frac{(\alpha\hat{a}^\dagger)^n}{n!}|0\rangle \\
&= e^{-\frac{1}{2}|\alpha|^2} \sum_{n=0}^{\infty} \frac{\alpha^n}{n!} \sqrt{n!}|n\rangle \\
&= e^{-\frac{1}{2}|\alpha|^2} \sum_{n=0}^{\infty} \frac{\alpha^n}{\sqrt{n!}}|n\rangle,
\end{aligned} \tag{109}$$

which comparing to (103) immediately gives us the coherent state $|\alpha\rangle$. This mapping motivates the claim that $\hat{D}(\alpha)$ has the action of 'displacing' the ground state by α in phase-space. It turns out that this interpretation is more powerful, and extends beyond just the ground state to any coherent state. In particular, we will now show that the displacement operator also obeys the group property [14] that for 2 consecutive displacements by α and β , $\hat{D}(\beta)\hat{D}(\alpha) = \hat{D}(\alpha + \beta)$ up to an overall phase. A consequence of this relation is that by associativity, we can apply the displacement operation $\hat{D}(\beta)$ to any coherent state $|\alpha\rangle$ to obtain yet another coherent state $|\alpha + \beta\rangle$ [14].

Let $A \equiv \alpha\hat{a}^\dagger - \alpha^*\hat{a}$, $B \equiv \beta\hat{a}^\dagger - \beta^*\hat{a}$. Then by comparing to the form of $\hat{D}(\alpha + \beta)$ obtained from (99), we see that exponentiating $A + B = (\alpha + \beta)\hat{a}^\dagger - (\alpha + \beta)^*\hat{a}$ will yield the overall displacement we want to obtain. We therefore want to show that $\exp(B)\exp(A) = \exp(A + B)$ up to some global phase in order to prove the required group relation. The BCH formula (105) tells us immediately that this will hold if the commutator $[A, B]$ is proportional to the identity:

$$\begin{aligned} [A, B] &= [\alpha\hat{a}^\dagger - \alpha^*\hat{a}, \beta\hat{a}^\dagger - \beta^*\hat{a}] \\ &= -\alpha\beta^*[\hat{a}^\dagger, \hat{a}] - \alpha^*\beta[\hat{a}, \hat{a}^\dagger] \\ &= 2i\text{Im}(\alpha\beta^*)\mathbb{I} \\ &\propto \mathbb{I}, \text{ as required.} \end{aligned} \tag{110}$$

We have shown that the displacement operator $\hat{D}(\alpha)$ has the effect of mapping the ground state to the coherent state $|\alpha\rangle$, and by extension, will map any coherent state $|\beta\rangle$ to the coherent state $|\alpha + \beta\rangle$ up to global phase. From (102), we therefore obtain a useful geometric interpretation of $\hat{D}(\alpha)$ as a pure displacement of the phase-portraits for each case by the vector α in the complex plane.

It would be nice if this pure displacement picture extended beyond coherent states to any arbitrary state in the Hilbert space. Unfortunately, the presence of the global phase in the group relation $\hat{D}(\beta)\hat{D}(\alpha) = \hat{D}(\alpha + \beta)e^{i\phi(\alpha, \beta)}$ means that this will not hold exactly, as we find that for a general non-coherent state, the displacement operation will also have the result of deforming its phase-portrait in phase-space. However, for certain mathematical objects, the pure displacement interpretation will still hold for any arbitrary state. In particular, [14] discusses how the pure displacement picture still holds when considering quasi-probability distributions for the motional state, such as the Wigner function, or P and Q functions. These functions are not considered here, however, we will also find in the following that for the specific case of expectation values of position and momentum that we are interested in, the pure displacement interpretation of the operator $\hat{D}(\alpha)$ will indeed extend to any state in the space. An easy way to demonstrate this is by considering explicitly the form of the creation and annihilation operators in the displaced frame:

$$\hat{D}^\dagger(\alpha)\hat{a}\hat{D}(\alpha) = \exp(\alpha^*\hat{a} - \alpha\hat{a}^\dagger) \hat{a} \exp(\alpha\hat{a}^\dagger - \alpha^*\hat{a}) \tag{111}$$

By application of the Campbell identity (80):

$$\begin{aligned} \hat{D}^\dagger(\alpha)\hat{a}\hat{D}(\alpha) &= \hat{a} + [\alpha^*\hat{a} - \alpha\hat{a}^\dagger, \hat{a}] + \dots \\ &= \hat{a} - \alpha[\hat{a}^\dagger, \hat{a}] + \dots \\ &= \hat{a} + \alpha, \end{aligned} \tag{112}$$

where higher order commutators in the expansion have vanished as these all contain nested commutators with the identity $[\hat{a}, \hat{a}^\dagger] = \mathbb{I}$. Similarly, for \hat{a}^\dagger :

$$\begin{aligned}
\hat{D}^\dagger(\alpha)\hat{a}^\dagger\hat{D}(\alpha) &= \hat{a}^\dagger + [\alpha^*\hat{a} - \alpha\hat{a}^\dagger, \hat{a}^\dagger] + \dots \\
&= \hat{a}^\dagger + \alpha^*[\hat{a}, \hat{a}^\dagger] + \dots \\
&= \hat{a}^\dagger + \alpha^*
\end{aligned} \tag{113}$$

From these identities, we can immediately obtain expectation values for the previously defined operators \hat{X}_1 and \hat{X}_2 for any arbitrary displaced state $\hat{D}(\alpha)|\psi\rangle$. Defining $\langle\hat{X}_1\rangle_{D_\alpha\psi}$ as the expectation of \hat{X}_1 for the displaced state, and $\langle\hat{X}_1\rangle_\psi$ for the undisplaced state (and analogously for \hat{X}_2), we obtain:

$$\begin{aligned}
\langle\hat{X}_1\rangle_{D_\alpha\psi} &= \langle\psi|\hat{D}^\dagger(\alpha)\hat{X}_1\hat{D}(\alpha)|\psi\rangle \\
&= \frac{1}{2}\langle\psi|\hat{D}^\dagger(\alpha)(\hat{a} + \hat{a}^\dagger)\hat{D}(\alpha)|\psi\rangle \\
&= \frac{1}{2}\langle\psi|(\hat{a} + \alpha + \hat{a}^\dagger + \alpha^*)|\psi\rangle \\
&= \langle\psi|\frac{1}{2}(\hat{a} + \hat{a}^\dagger)|\psi\rangle + \langle\psi|\text{Re}(\alpha)|\psi\rangle \\
&= \langle\hat{X}_1\rangle_\psi + \text{Re}(\alpha)
\end{aligned} \tag{114}$$

$$\begin{aligned}
\langle\hat{X}_2\rangle_{D_\alpha\psi} &= \langle\psi|\hat{D}^\dagger(\alpha)\hat{X}_2\hat{D}(\alpha)|\psi\rangle \\
&= \frac{1}{2i}\langle\psi|\hat{D}^\dagger(\alpha)(\hat{a} - \hat{a}^\dagger)\hat{D}(\alpha)|\psi\rangle \\
&= \frac{1}{2i}\langle\psi|(\hat{a} + \alpha - \hat{a}^\dagger - \alpha^*)|\psi\rangle \\
&= \langle\psi|\frac{1}{2i}(\hat{a} - \hat{a}^\dagger)|\psi\rangle + \langle\psi|\text{Im}(\alpha)|\psi\rangle \\
&= \langle\hat{X}_2\rangle_\psi + \text{Im}(\alpha)
\end{aligned} \tag{115}$$

Thus, when considering only expectation values of position and momentum, we recover the 'pure displacement' interpretation for any arbitrary state $|\psi\rangle$ in the motional space. This justifies the interpretation of $\alpha(t)$ for a displacement by $\hat{D}(\alpha(t))$ as giving the 'phase-space trajectory' of the phonon states irrespective of the initial state. Note this interpretation can be a little misleading, as care must be taken when considering the resulting wavefunction as a whole, which in general will be deformed as a result of the operation.